

# Expanding Three-Coordinate Gold(I) Anticancer Agent Chemical Space

Charles E. Greif, Owamagbe N. Orobator, Chibuzor Olelewe, Sean Parkin, and Samuel G. Awuah\*



Cite This: <https://doi.org/10.1021/acs.jmedchem.5c00608>



Read Online

ACCESS |



Metrics & More

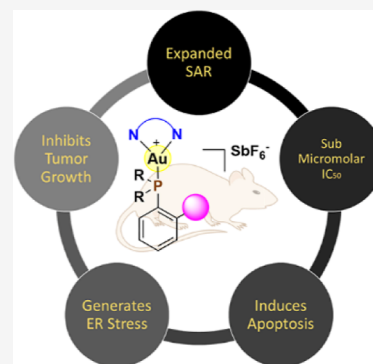


Article Recommendations



Supporting Information

**ABSTRACT:** We report the synthesis and characterization of 14 complexes of the type  $(\text{Au}(\text{R})[\text{NN}])^+$ , where R = tunable biaryldialkyl phosphine ligands and  $[\text{NN}]$  = bidentate phenanthroline derivatives as anticancer agents. These novel tricoordinate Au(I) complexes were characterized and evaluated in metabolically differentiated triple negative breast cancer (TNBC) cell lines for their cytotoxicity potential. The complexes demonstrated submicromolar cytotoxic activity against human breast cancer cells MDA-MB-231 or MDA-MB-468 with  $\text{IC}_{50}$ 's in the range of 0.4–5.0  $\mu\text{M}$ . Complex **2e** shows high potency in vitro and decreases 3D-breast cancer mammosphere viability. Mechanistic studies show **2e** promotes cell death by apoptosis with plausible mode of action via endoplasmic reticulum stress induction. Tumor growth inhibition in a metastatic TNBC mouse model was observed, demonstrating **2e**'s translational capability. We show for the first time the in vivo anticancer potential of a phosphine-supported tricoordinate-Au(I) complex in mice with suitable tolerability. These studies further expand the therapeutic potential of tricoordinate-Au(I) complexes.



## INTRODUCTION

Chemical space diversity of gold-derived complexes holds transformative impact in catalysis, electronics material chemistry, polymer science, and biomedicine. Descriptors such as redox potential, ligand tuning, geometry, and oxidation states have the potential to affect therapeutic utility in cancer treatment. Although platinum(II) agents are known first-line treatment options in cancer therapy, acquired platinum-resistance and toxic side effects remain a significant clinical problem.<sup>1,2</sup> Therefore, novel metal-based therapeutics including gold (Au) are needed to circumvent these limitations. It is worth noting that several transition metals have been deployed as anticancer agents, including iridium, osmium, copper, ruthenium, rhenium, titanium, palladium, technetium, and gold.<sup>3–25</sup> Many of which work via chemoselective and regioselective modification of biomolecules, redox activation, and photosensitization.<sup>26–31</sup> Energized by the approval of the anti-inflammatory drug auranofin,<sup>12</sup> increased work to understand the mechanism of Au anticancer action and has shown treatment with cationic gold complexes lead develop novel Au complexes continues to escalate.<sup>14,32–49</sup> Conventionally, Au anticancer agents are known to inhibit thioredoxin reductase (TrxR), of which many cancers overexpress.<sup>17,18,20</sup> Recent work from our laboratory and others is defining novel targets including distinct mitochondrial locales based on structure.<sup>11,21,50–58</sup>

Gold(I) complexes commonly bond in a linear fashion due to relativistic effects, one of which being the diminished energy gap between the 6s and 5d orbitals. Compared to the isoelectronic neighbors Pt(0) and Ag(I), Au(I) forms linear

two-coordinate complexes at a much higher rate, with the others forming complexes in higher coordination numbers. That is not to say that gold(I) complexes with a higher valence are impossible; they can be synthesized, leading to three-coordinate trigonal planar or even four-coordinate tetrahedral and square planar compounds.<sup>59–61</sup> Seminal work from Vicente, Usón, Laguna, and Jones provide an excellent starting point for conceptualizing these uncommon tri- and tetra-coordinate complexes.<sup>62–64</sup> Bourissou expanded on this work, synthesizing Au(I) three-coordinate boratranes, and also synthesizing a redox active Au(I)/Au(III) complex that forms a three-coordinate complex in situ.<sup>65–69</sup> The potency of two-coordinate linear Au(I) complexes were shown by Che, but three-coordinate trigonal planar Au(I) complexes were only recently probed by our research group.<sup>11,58,70,71</sup>

Following initial work that introduced tricoordinate Au(I) complexes in biology, we envisioned that expanding the Au(I) chemical library with unique trigonal geometric will convey new mechanisms and potency for disease treatment. We capitalized on the biological compatibility of phosphines as useful monodentate ancillary ligands for this work. Biaryldialkyl phosphines ligands have been utilized as cocatalysts in

**Received:** March 1, 2025

**Revised:** June 18, 2025

**Accepted:** July 4, 2025



ACS Publications

© XXXX The Authors. Published by  
American Chemical Society

A

<https://doi.org/10.1021/acs.jmedchem.5c00608>  
J. Med. Chem. XXXX, XXX, XXX–XXX

several palladium catalytic cross-coupling reactions including Suzuki–Miyaura and Negishi cross coupling reactions.<sup>72–78</sup> The structural variations within the selected phosphine ligands with various electron withdrawing groups that affect reactivity of the Au center is particularly attractive for medicinal structure activity relationship studies.<sup>79</sup> They are electron rich, hemilabile ligands that help stabilize the catalyst intermediate. These ligands are both easy to synthesize and easy to tune, making them an ideal candidate for SAR studies.

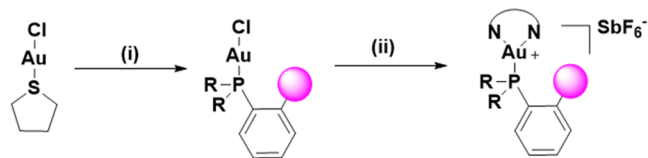
Triple negative breast cancers (TNBCs) are incredibly aggressive cancers that are more prevalent in younger women or women of African or Hispanic descent.<sup>80</sup> They lack the overexpression of human epidermal growth factor receptor 2 (HER2), estrogen, and progesterone. Mutations of the BRCA genes are genetic indicators of a predisposition to TNBCs.<sup>81,82</sup> Many compounds used to quell metastatic TNBCs target mechanistic pathways, such as PARP inhibitors (Olaparib) or PD-L1 inhibitors (durvalumab).<sup>83,84</sup> However, due to the complicated genetic abnormalities and aggressive nature of TNBCs, there's a great need for additional chemotherapeutics.

Here, we report the facile synthesis of 15 cationic tricoordinate Au(I) complexes for the use as anti-TNBC agents. The lead complex, AuTri-Phos 2e, was chosen after spectroscopic characterization, and photophysical, stability, and cytotoxicity studies. The complex induces apoptosis in TNBC and was found to increase lipid accumulation and alter the expression of proteins related to endoplasmic reticulum stress conditions. The complex not only inhibits 3D-mammosphere proliferation, but also halts tumor initiation, and significantly inhibits tumor growth with appreciable tolerable in vivo.

## RESULTS AND DISCUSSION

**Synthesis and Characterization.** Expanding on work previously described by our lab,<sup>58</sup> we postulate that Au(I) biaryldialkyl phosphines, commonly used in catalytic systems, and [N<sup>^</sup>N] bidentate donor ligands will act as the building block for our cationic tricoordinate system. These compounds contain N–Au bond lengths that differ in length. We posit that complexes with longer N–Au bond lengths are slightly more labile allowing for potential biological reactions to occur. The biaryldialkyl phosphine donor ligands are desirable for this system due to their functionalization possibilities. Preparation of these complexes, herein called AuTri-Phos, are straightforward and scalable, as shown in Scheme 1. Synthesis of the complexes followed established literature procedure via chloride abstraction and silver transmetalation of [N<sup>^</sup>N]-bidentate donor ligands with respective Au(I) centers, leading to the desired cationic complex in moderate to high yields. Structures of several complexes were ascertained via X-ray

**Scheme 1. Synthetic Route of AuTri-Phos 1a–f, 2a–e, and 3b, 3d, and 3f<sup>a</sup>**



<sup>a</sup>Reagents and conditions: (i) X-, C-, or JohnPhos, DCM, rt, 1 h, 60–70%; (ii) AgSbF<sub>6</sub>, [N<sup>^</sup>N]-bidentate ligand,\* DCM, rt, 30 min, 41–81%. \*[N<sup>^</sup>N]-bidentate ligands can be reviewed in Table 2.

crystallography (Figures S1–S11). The complexes were characterized via <sup>1</sup>H NMR, <sup>13</sup>C NMR, <sup>31</sup>P NMR, and purity was determined via elemental analysis (Figures S12–S41).

**X-ray Crystallography.** Single crystals of compounds AuTri-Phos 1c–f and 2c were grown via either recrystallization using acetonitrile or vapor diffusion of diethyl ether into an aliquot of compound dissolved in DCM for analysis by X-ray diffraction. The solved crystal structures all showed the distorted tricoordinate motif unique for these Au(I) complexes containing [N<sup>^</sup>N]-bidentate donor ligands and monodentate phosphorus ligands. The Au–N bond lengths differ for all these complexes, with the Au–N1 bond being much shorter and stronger (2.1441–2.2251 Å) compared to the other longer, more labile Au–N2 bond (2.4756–2.623 Å, Table 1). We see a strong, stable Au–P bond length (2.2332–2.2421 Å) for all solved complexes. Most of these complexes are oriented in the triclinic *P*1 space group, with exceptions being 1c (monoclinic *P*<sub>2</sub><sub>1</sub>/*m*) and 1e (monoclinic *P*<sub>2</sub><sub>1</sub>/*n*). The bond angles deviate from the idealized trigonal planar geometry because of the lability of the Au–N2 bond. We see a much smaller bond angle between the N1–Au–N2 (69.27–70.01°) than expected, which is counterbalanced by the much larger N1–Au–P bond angle (154.46–166.03°). The full X-ray characterization tables are provided in the Supporting Information (Tables S1–S5).

**Solution Stability and Photophysical Properties.** The solution behavior and stability of the complexes was investigated via detailed spectroscopic and absorbance analyses. The study was initiated by UV–vis absorbance characterization after dissolution of complexes in DCM to determine the absorbance profile of the complexes. The UV–vis absorbance profile (Figures 1A and S62–S78) show λ<sub>max</sub> ranging from 262 to 286 nm depending on ancillary ligands, with the complexes containing the DPPZ [N<sup>^</sup>N] bidentate donor ligand having two additional broad peak ranging from 360 to 370 nm and 378 to 388 nm. We then sought to determine the stability profile of the complexes in physiologically relevant media, hypothesizing that complex stability is correlated to in vitro potency. The UV–vis absorption profile in Dulbecco's modified Eagle's medium (DMEM) shows little alteration over 25 h for complexes containing either the bathophenanthroline or 4,7-dimethylphenanthroline ligand (Figures 1A and S65–S78). However, other complexes in the AuTri-Phos series proved unstable in DMEM in a time-dependent manner. This led us to narrow our evaluation to exclude compounds containing other [N<sup>^</sup>N]-bidentate ligands.

We then sought to determine which complexes show higher accumulation in whole cell settings in MDA-MB-468 cells. We treated the 468 cells with 10 μM of 1c, 1e, 2c, and 2e for 18 h and measured the intracellular accumulation. We see that complexes containing the more sterically hindered bathophenanthroline bidentate ligand have lower cellular uptake when compared to their 4,7-dimethyl phenanthroline counterpart. This could be due to an increased lipophilicity because of the additional phenyl rings. There appears to be some effect when considering the p-ancillary ligands, but more complexes need to be studied before making a definite conclusion (Figure 1B).

**Lead Complex Identification and Stability with Biological Reductants.** We know from previous work performed in our lab that these complexes containing biaryldialkyl phosphines perform well in TNBCs, and we expect these complexes to work similarly. We evaluated this

Table 1. Selected Bond Lengths and Angles for AuTri-Phos Complexes

compound	bond lengths (Å)			bond angles (°)		
	N <sub>1</sub> –Au	N <sub>2</sub> –Au	P–Au	N <sub>1</sub> –Au–P	N <sub>2</sub> –Au–P	N <sub>1</sub> –Au–N <sub>2</sub>
AuTri-Phos 1c	2.2251(18)	2.4756(19)	2.2400(7)	154.46(6)	134.82(5)	69.86(10)
AuTri-Phos 1d	2.153(2)	2.623(2)	2.2421(8)	166.03(7)	125.05(6)	68.72(9)
AuTri-Phos 1e	2.1460(15)	2.6054(15)	2.2415(4)	164.78(4)	125.70(3)	69.27(5)
AuTri-Phos 1f	2.1441(17)	2.5823(17)	2.2347(5)	163.59(5)	125.33(4)	70.01(6)
AuTri-Phos 2c	2.178(3)	2.538(4)	2.2332(10)	155.74(11)	134.54(10)	69.54(12)

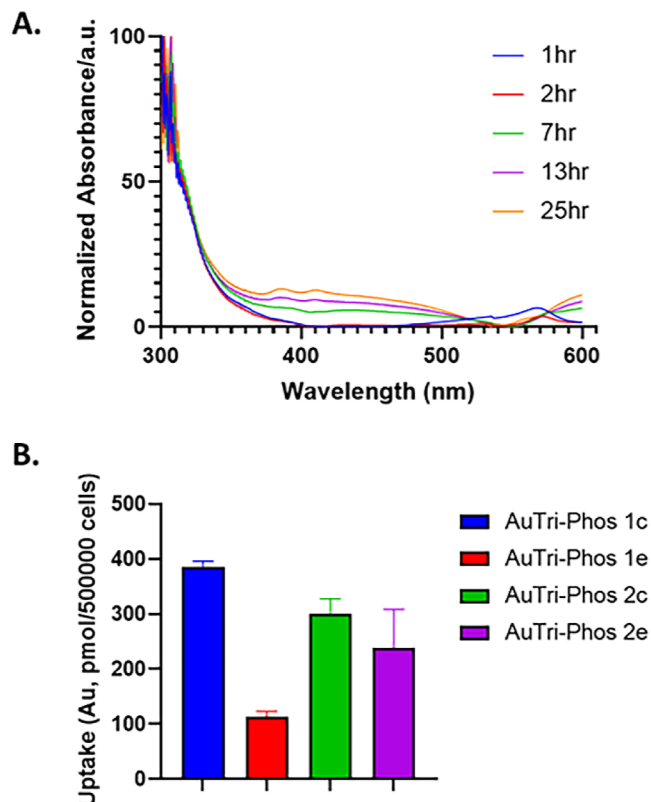


**Figure 1.** (A) UV-vis spectra of AuTri-Phos 2e in DMEM over 25 h. (B) Whole cellular uptake of AuTri-Phos 1c, 1e, 2c, and 2e complexes in MDA-MB-468 TNBC cells. Cells treated at a concentration of 10  $\mu$ M for 18 h and analyzed by ICP-MS. Data plotted as mean  $\pm$  s.e.m. ( $n = 2$ ).

library of complexes in MDA-MB-231 and -468 TNBC cell lines via MTT (Table 2). The complex 2e exhibited submicromolar IC<sub>50</sub> values, and was chosen as our lead complex due to this potency and previously mentioned solution stability.

We evaluated the biological stability of 1c, 1e, 2c, and 2e by monitoring the change in NMR signals after reacting with L-GSH, a known biological reductant (Figures 2A and S62–S64). If the compound has off-target effects, that could impact the potency of the complex. Following the addition of L-GSH to complex 2e the proton resonances of 2e in the aromatic region slightly shifted downfield and remained unchanged throughout the 25 h time course. We did not observe any purple coloration of the NMR tube to suggest gold reduction. This may be indicative of solution stability of 2e.

Finally, we measured the change in absorbance of 2e in the presence of the protein bovine serum albumin (BSA). Au(I) complexes have a propensity to react with proteins containing the amino acid cysteine, due to gold's affinity for thiol

containing complexes. BSA contains 17 cysteines, 16 of which participate in S–S disulfide bonding for stability purposes. If 2e reacts with BSA, it could lead to a denaturing of the protein and various undesirable side effects. The slight baseline deviation observed in the wavelength range of 600–400 nm in Figure 2B, may be attributable to adduct formation or Au(I) reduction. However, there was no observable purple coloration of the solution or cuvette often associated with reduced gold.

**AuTri-Phos Complexes Inhibit Triple Negative Breast Cancer Growth and Proliferation.** We examined the efficacy of 2e in 3-dimensional TNBC mammosphere growth and proliferation due to the submicromolar cytotoxicity of 2e in monolayer MDA-MB-468. As mammospheres are more representative of live tumors than monolayers, they provide a deeper understanding of in vitro potency.<sup>85</sup> In ultra-low attachment surface 24-well plates, MDA-MB-468 cells were plated 4000 cells/well. Cells were left to adhere and grow for 2 days into small spheroids, after which the spheroids were treated in a concentration dependent manner. After 5 days of treatment, we see 2e significantly decreases the size and quantity of mammospheres compared to the control (Figure 3A).

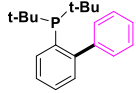
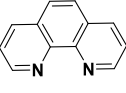
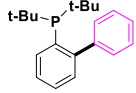
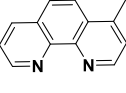
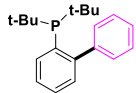
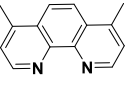
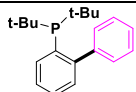
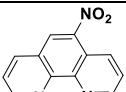
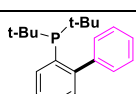
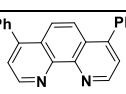
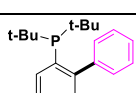
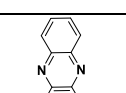
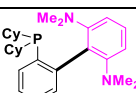
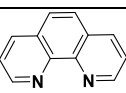
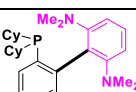
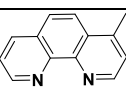
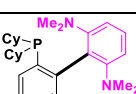
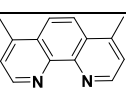
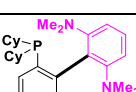
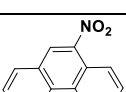
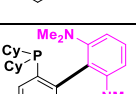
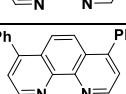
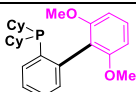
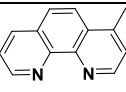
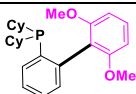
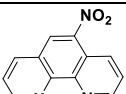
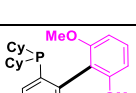
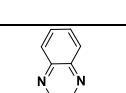
**AuTri-Phos 2e Induces Apoptosis in Triple Negative Breast Cancer.** We sought to identify to mechanism of cell death through fluorescence-assisted cell sorting (FACS). Au(I) complexes are known to induce cell death in a variety of ways, most notably mitophagy via mitochondrial stress and autophagy via apoptosis. We sought to narrow down the possible cell death pathways to glean greater insight in to the mechanism. Exposing the TNBC cell line MDA-MB-468 to 2  $\mu$ M of 2e, we found a significant increase in apoptotic cells compared to the control (97.8% vs 9.29%, Figure 3C,D).

We further validated this mechanism by immunoblotting for the common apoptotic markers Caspase 3 and PARP. Cells that undergo apoptosis see a decrease in Caspase 3 and PARP, while seeing an increase in their cleaved counterparts. We see this aforementioned decrease and increase in protein concentration in a time-dependent manner, shown in Figure 2B.

We then determined the effect of 2e on tumor initiation, utilizing the 3-dimensional mammospheres once again. We plated MDA-MB-468 cells at 4000 cells/well in an ultra-low attachment surface 24-well plate, after which the cells were immediately treated with 2e in a concentration dependent manner. After 5 days of treatment, we see that, compared to the control, 2e significantly inhibits tumor initiation in 3-dimensional mammospheres (Figure 3A).

**Exploring Avenues of Apoptotic Cell Death.** We then sought to identify the mechanism of action of cell death by probing mitochondrial stress pathways. Previous work performed in our lab shows Au(I) complexes perturb mitochondrial function by disrupting mitochondrial bioenergetics and inducing mitochondrial reactive oxygen species

Table 2. Cell Viability of AuTri-Phos Complexes With Varied Ligands Expressed as IC<sub>50</sub> Values in TNBC after 72 h Treatment

Compound	Phosphine Ligand	[N <sup>N</sup> ]-bidentate ligand	Cell Line IC <sub>50</sub> (μM)	
			MDA-MB-231	MDA-MB-468
AuTri-Phos 1a			2.67 ± 0.13	1.51 ± 0.08
AuTri-Phos 1b			1.73 ± 0.11	0.75 ± 0.04
AuTri-Phos 1c			1.73 ± 0.10	0.45 ± 0.06
AuTri-Phos 1d			2.91 ± 0.09	0.84 ± 0.08
AuTri-Phos 1e			1.03 ± 0.07	0.62 ± 0.06
AuTri-Phos 1f			3.03 ± 0.07	2.37 ± 0.13
AuTri-Phos 2a			5.07 ± 0.12	2.50 ± 0.03
AuTri-Phos 2b			3.60 ± 0.11	1.13 ± 0.05
AuTri-Phos 2c			2.35 ± 0.07	0.80 ± 0.04
AuTri-Phos 2d			3.30 ± 0.07	1.02 ± 0.04
AuTri-Phos 2e			1.12 ± 0.06	0.63 ± 0.05
AuTri-Phos 3b			2.00 ± 0.07	0.91 ± 0.09
AuTri-Phos 3d			2.61 ± 0.08	1.13 ± 0.06
AuTri-Phos 3f			5.38 ± 0.10	4.60 ± 0.09



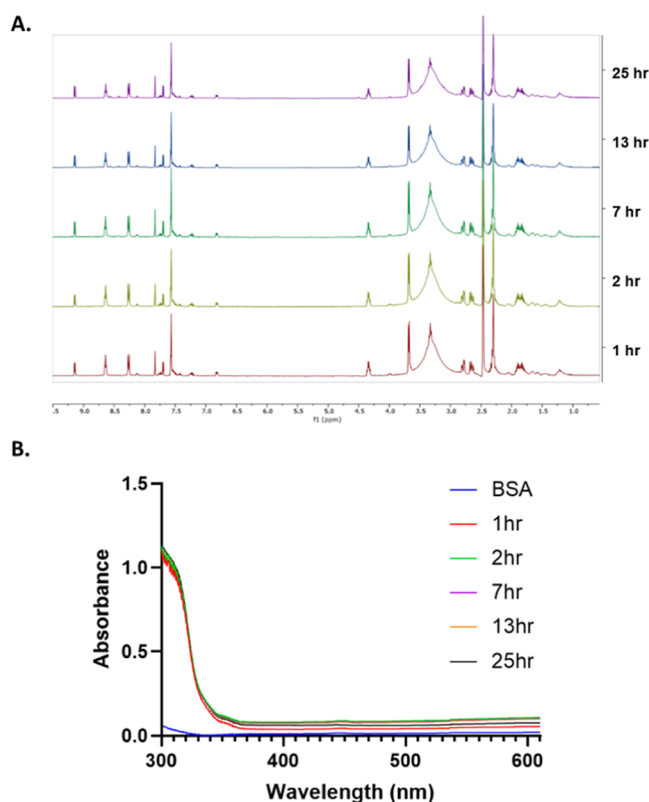


**Figure 2.** Solution stability. (A) Time dependent NMR studies of AuTri-Phos **2e** incubated with L-GSH at a 1:10 **2e**/L-GSH ratio. (B) UV-vis spectra of AuTri-Phos **2e** incubated with BSA at a 1:10 **2e**/BSA ratio.

(mtROS). To confirm the expected target of mitochondrial function, we evaluated the effect of **2e** on the mtROS of the 468 cells. We know that heightened ROS accumulation can trigger apoptosis from previous work, and we hypothesized the increase in apoptotic cells were due to this accumulation. We utilized the MitoSOX red dye to detect superoxide production. When the MitoSOX dye is exposed to superoxide, the complex is oxidized and produces a bright red fluorescence, which we monitored using FACS. We treated MDA-MB-468 cells at 2  $\mu$ M and 5  $\mu$ M concentrations. Surprisingly, we saw no significant change in mtROS after treatment (Figure 4A). We then probed mitochondrial fusion and fission proteins to determine if the complex was affecting mitochondrial generation. We see a decrease in MFN1, a mitochondrial fusion protein. However, other fusion and fission proteins have little change (Figure 4B). With this in mind, we chose to evaluate mitochondrial bioenergetics, utilizing the Seahorse XF analyzer to perform a MitoStress test on the MDA-MB-468 cell line to measure oxygen consumption rate (OCR). The evaluation first involves a pneumatic injection of **2e** in wells containing the TNBC cells, followed by injection of known electron transport chain (ETC) inhibitors (Figure 4C). Curiously, we see that **2e** increases OCR, which is typical for ETC uncoupling agents. We see an increase in basal and metabolic respiration, and no real effect on ATP production (Figure 4D–F).

Given this conundrum, we searched for additional avenues of cell death. Previous work has shown that gold nanoparticles can induce apoptosis by affecting the endoplasmic reticulum (ER).<sup>86,87</sup> Additional research has shown the mitochondria

and ER rely on each other to maintain cellular homeostasis.<sup>88</sup> When the ER is stimulated due to mitochondrial perturbation or other stress avenues, internal homeostasis is disrupted due to the increase in misfolded proteins.

This can lead to the activation of Caspase 3, which causes downstream cleaving of PARP.<sup>89</sup> This is consistent with what we found in our apoptosis studies. With this in mind, we hypothesized AuTri-Phos **2e** causes ER stress which then leads to apoptosis. We first examined the effect of **2e** on lipid accumulation in the cells, as this can be directly related to ER stress.<sup>90,91</sup> We utilized the Oil Red O (ORO) lipid staining dye to determine the change before and after treatment. When the endoplasmic reticulum becomes overstimulated, it responds by overproducing lipids and releasing them into the cytosol. The ORO dye is fat soluble and will selectively bind to lipids and triglycerides in cells and tissues and stain them red when observed under confocal microscope, making it ideal for our purposes. We hypothesize that as the ER becomes stressed due to treatment with our lead complex, we will see an increase in lipid accumulation.

We treated MDA-MB-468 cells with 2  $\mu$ M of **2e**, after which we fixed the cells and stained both the nucleus with a working concentration of Hoescht dye and the lipids with a working concentration of ORO dye. Using fluorescence microscopy, we see a clear increase in lipid accumulation in the treated cells (Figure 5A). We then evaluated the expression of different ER stress related proteins via immunoblotting. We see a clear increase in proteins involved in the PERK-eIF2 $\alpha$ -C/EBP-homologous protein pathway, prompting us to believe that AuTri-Phos **2e** is causing ER stress, which leads to apoptosis (Figure 5B).

**In Vivo Anticancer Activity.** To determine the in vivo antitumor efficacy of Au-Tri Phos **2e**, mouse models of TNBC developed by inoculating Balb/c mice with 4T1 cells were treated with 10 mg kg<sup>-1</sup> of Au-Tri Phos **2e** intraperitoneally three times a week. A control group ( $n = 5$  mice) was administered the vehicle containing 1% DMSO, 37.5% kolliphor, 37.5% ethanol, and 24% deionized water. The Au-Tri Phos **2e** treated group showed significant tumor growth suppression (Figure 6A,B) and stable body weight (Figure 6C) compared to the control group. This indicates that Au-Tri Phos **2e** is a tolerable and potent antitumor agent. We further conducted Au biodistribution studies to determine the Au content across different organs. This analysis shows a significant accumulation of gold in the liver, kidney, and spleen (Figure 6D). The high Au contents in the liver, kidney, and spleen indicate the active metabolic, excretory, and reticuloendothelial roles, respectively, of these organs in Au clearance. Furthermore, histological analysis using hematoxylin and eosin staining of tissue slices revealed a significant reduction of tumor cellularity in the Au-Tri Phos **2e** treated group compared to the control group (Figure 6E). However, there was no marked difference between the cellularity of the lungs, liver, kidney, spleen, and heart tissues of the treated and control groups (Figure 6E). Taken other, the in vivo studies demonstrate the antitumor efficacy and promising safety profile of Au-Tri Phos **2e**.

## CONCLUSION

Building upon work previously performed in our lab, we described SAR studies on a small library of cationic tricoordinate Au(I) complexes. These complexes utilize the easily tunable biaryldialkyl phosphine ligand, which contains

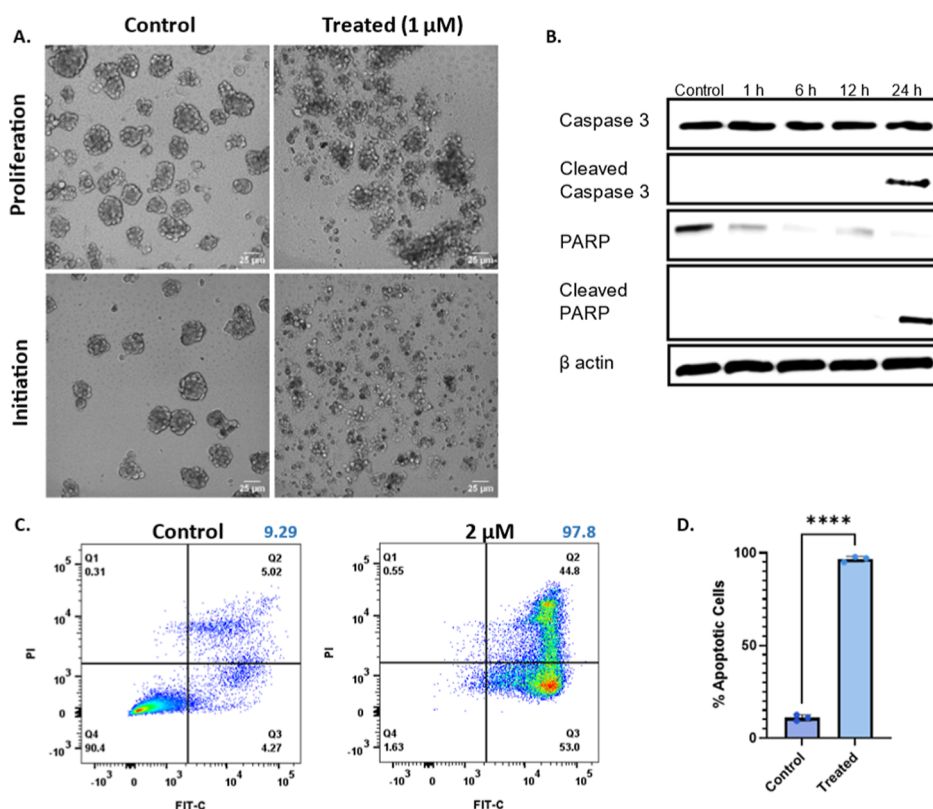


**Figure 3.** Apoptosis evaluation. (A) Light microscopy images of 3D-mammospheres before and after treatment. Data presented in (B) was analyzed via one-way ANOVA ( $***p < 0.0001$ ). (B) Immunoblotting of apoptotic related proteins in MDA-MB-468. Full unedited blots can be found in Figure S80. (C,D) Flow cytometry analysis of the apoptotic effect of AuTri-Phos 2e. (C) Immunoblotting of apoptotic related proteins in MDA-MB-468.

varying levels of electron density, coupled with electron rich 1,10-phenanthroline derivatives. When taking into account the potency, whole cell uptake, and overall solution stability, AuTri-Phos 2e was clearly the complex with the most potential. We found that this complex inhibited 3D-breast stem cell growth and proliferation. Flow cytometry shows a clear increase in apoptotic cells after treatment with 2 μM of the complex, with immunoblotting confirming this hypothesis. The Oil Red O ER stress assay shows a drastic increase in lipid accumulation, and immunoblotting of relevant apoptotic and ER stress proteins show a time-dependent change in expression consistent with ER stress related apoptosis. Finally, we see impressive tolerability in the murine model, while also seeing significant inhibition of tumor proliferation. While work is ongoing to further expand the library, our current findings highlight the potential of this novel library of tricoordinate Au(I) complexes for work in cancer immunotherapy.

## EXPERIMENTAL PROCEDURES

**General Information.** Solvents used in this work were purchased from Pharmco-Aaper (ACS grade), and they were used as purchased.  $\text{HAuCl}_4 \cdot 3\text{H}_2\text{O}$  was purchased from Nano Partz and stored under a nitrogen atmosphere. Bathophenanthroline was purchased from TCI. Silver hexafluoroantimonate was purchased from Oakwood chemicals. 1,10-Phenanthroline, 4-methyl-1,10-phenanthroline, 4,7-dimethyl-1,10-phenanthroline, 5-nitro-1,10-phenanthroline, JohnPhos, CPhos, and SPhos were purchased from AmBeed. 3-(4,5-Dimethylthiazol-2-yl)-2,5-diphenyltetrazolium bromide (MTT) was purchased from Cayman Chemicals.  $\text{AuCl}_3\text{JohnPhos}$ ,  $\text{AuCl}_3\text{CPhos}$ , and  $\text{AuCl}_3\text{SPhos}$  were synthesized according to the reported procedure.<sup>58</sup> Deuterated solvents were purchased from Cambridge Isotope Laboratories

(Andover, MA). NMR spectra were recorded on a Bruker Avance NEO 400 MHz spectrometer and 500 MHz JEOL ECZr. Samples were calibrated for  $^1\text{H}$  NMR ( $\text{CD}_3\text{CN}$   $\delta = 1.94$  ppm,  $\text{CD}_2\text{Cl}_2$   $\delta = 5.32$  ppm),  $^{13}\text{C}$  ( $^1\text{H}$ -decoupled) NMR ( $\text{CD}_3\text{CN}$   $\delta = 118.26$ , 1.32 ppm,  $\text{CD}_2\text{Cl}_2$   $\delta = 53.84$  ppm), and  $^{31}\text{P}$  ( $^1\text{H}$ -decoupled) NMR externally referenced to  $\text{H}_3\text{PO}_4$  ( $\delta = 0.00$ ). Elemental analysis results were obtained from Atlantic Microlabs, Inc. (Norcross, GA). Fluorescent images were obtained from a fluorescence microscope in total internal reflection fluorescence (TIRF) and epifluorescence mode using 488 and 510 nm laser excitation, power 1 mW/cm<sup>2</sup> exposure time of 200 ms using a 20× air objective. Images were processed with ImageJ software. Purity of compounds synthesized were ascertained by elemental analysis with purity >95%.

**Synthesis and Characterization. General Procedure for the Preparation of AuTri-Phos Compounds.** In a 50 mL round-bottom flask with a stir bar, 1 mol eq of [ $\text{N}^{\wedge}\text{N}$ ] bidentate ligand and 1.1 mol eq of silver hexafluoroantimonate were added and dissolved in 4 mL dichloromethane (DCM). In a 5 mL borosilicate scintillation vial, 1 mol eq of  $\text{AuCl}_3$ -phosphate was dissolved in 2 mL DCM. The Au solution was added dropwise to the solution containing the silver salt and bidentate ligand, after which the round-bottom flask was wrapped in aluminum foil and left to stir for 30 min. The solution was collected, centrifuged, decanted, and reduced to minimum volume, after which diethyl ether was added to precipitate out the desired complex. The complex was dried on a high pressure vacuum overnight and characterization was performed the following day.

**Synthesis of AuTri-Phos 1a.** Prepared as described in the general procedure.  $\text{AuCl}_3\text{JohnPhos}$  (100 mg, 0.1884 mmol), silver hexafluoroantimonate (71.2 mg, 0.2072 mmol), and 1,10-phenanthroline (34 mg, 0.1884 mmol). Yield: 96.7 mg, 56%.  $^1\text{H}$  NMR (400 MHz,  $\text{CD}_3\text{CN}$ ,  $\delta$ ): 8.86 (s, 1H), 8.71 (d,  $J = 8$  Hz, 2H), 8.16 (s, 2H), 8.13 (d,  $J = 8$  Hz, 1H), 8.01 (quart,  $J = 16$  Hz, 2H), 7.625 (quint,  $J = 36$  Hz, 2H), 7.185 (t,  $J = 12$  Hz, 1H), 7.10 (d,  $J = 8$  Hz, 2H), 6.30 (s, 2H), 5.78 (s, 1H), 1.59 (s, 9H), 1.55 (s, 9H);  $^{13}\text{C}$  NMR (101 MHz,

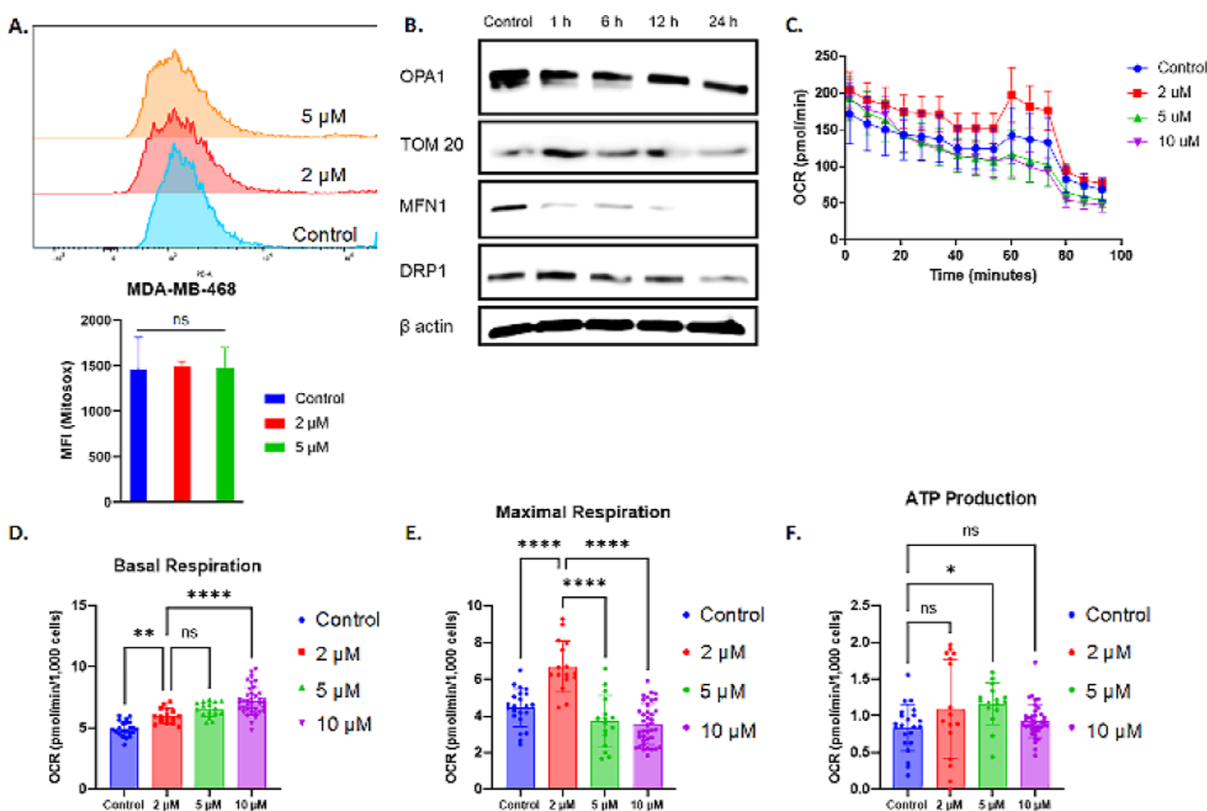


**Figure 4.** Evaluation of mitochondrial assays. (A) Flow cytometry analysis on the production of mitochondrial reactive oxygen species of AuTri-Phos **2e**. (B) Immunoblotting of mitochondria fusion and fission related proteins in MDA-MB-468. Full unedited blots can be found in Figure S80. (C) Seahorse bioenergetic stress test of AuTri-Phos **2e**. (D–F) Extrapolated data from the bioenergetic stress test. Data was analyzed via one-way ANOVA (\* $p < 0.05$ , \*\* $p < 0.01$ , \*\*\*\* $p < 0.0001$ . ns = not significant).

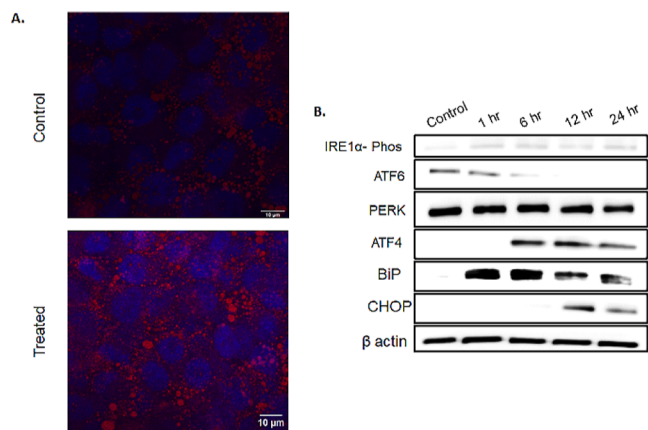


**Figure 5.** Endoplasmic reticulum stress evaluation. (A) Fluorescence microscopy images of MDA-MB-468 cells after treatment with AuTri-Phos **2e** and staining via Hoechst and ORO dyes. (B) Immunoblots showing the change in expression of endoplasmic reticulum proteins after treatment with **2e** in a time-dependent manner.

$\text{CD}_3\text{CN}$ ,  $\delta$ ): 151.63, 142.67, 139.80, 134.52, 133.57, 133.50, 131.39, 130.76, 129.72, 128.05, 127.98, 125.59, 38.07, 37.82, 30.70, 30.63;  $^{31}\text{P}$  NMR (161.9 MHz,  $\text{CD}_3\text{CN}$ ,  $\delta$ ): 59.90;  $^{19}\text{F}$  NMR (376 MHz,  $\text{CD}_3\text{CN}$ ,  $\delta$ ): -111.11, -116.23, -121.41, -126.55, -131.69, -136.82.

**Synthesis of AuTri-Phos 1b.** Prepared as described in the general procedure. AuCl<sub>3</sub>JohnPhos (100 mg, 0.1884 mmol), silver hexafluoroantimonate (71.2 mg, 0.2072 mmol), and 4-methyl-1,10-phenanthroline (36.6 mg, 0.1884 mmol). Yield: 107.2 mg, 62%.  $^1\text{H}$  NMR (400 MHz,  $\text{CD}_3\text{CN}$ ,  $\delta$ ): 8.89 (s, 1H), 8.695 (t,  $J = 16$  Hz, 2H) 8.34 (d,  $J = 8$  Hz, 1H), 8.18 (d,  $J = 16$  Hz, 1H), 8.14 (d,  $J = 8$  Hz, 1H),

8.01 (q,  $J = 16$  Hz, 1H), 7.865 (d,  $J = 2$  Hz, 1H), 7.68–7.59 (m, 2H), 7.195 (t,  $J = 12$  Hz, 1H), 7.11 (d,  $J = 8$  Hz, 2H), 6.30 (t,  $J = 16$  Hz, 2H), 5.79 (t,  $J = 16$  Hz, 1H), 2.95 (s, 3H), 1.60 (s, 9H), 1.56 (s, 9H);  $^{13}\text{C}$  NMR (101 MHz,  $\text{CD}_3\text{CN}$ ,  $\delta$ ): 151.30, 143.76, 139.44, 134.53, 133.57, 133.50, 131.33, 129.69, 128.01, 127.95, 127.82, 127.82, 127.60, 126.33, 126.26, 125.46, 124.32, 38.06, 37.79, 30.72, 30.65;  $^{31}\text{P}$  NMR (161.9 MHz,  $\text{CD}_3\text{CN}$ ,  $\delta$ ): 60.03;  $^{19}\text{F}$  NMR (376 MHz,  $\text{CD}_3\text{CN}$ ,  $\delta$ ): -111.15, -116.27, -121.43, -126.56, -131.75, -136.87. Anal. Calcd:  $\text{C}_{41}\text{H}_{51}\text{AuF}_6\text{N}_4\text{PSb}$  C, 46.30%; H, 4.83%; N, 5.27%. Found:  $\text{C}_{41}\text{H}_{51}\text{AuF}_6\text{N}_4\text{PSb} \cdot 0.80\text{H}_2\text{O}$  C, 45.49%; H, 4.69%; N, 5.22%.

**Synthesis of AuTri-Phos 1c.** Prepared as described in the general procedure. AuCl<sub>3</sub>JohnPhos (100 mg, 0.1884 mmol), silver hexafluoroantimonate (71.2 mg, 0.2072 mmol), and 4,7-dimethyl-1,10-phenanthroline (39.2 mg, 0.1884 mmol). Yield: 112.9 mg, 64%.  $^1\text{H}$  NMR (400 MHz,  $\text{CD}_3\text{CN}$ ,  $\delta$ ): 8.66 (s, 1H), 8.33 (s, 2H) 8.13 (t,  $J = 16$  Hz, 1H), 7.82 (s, 2H), 7.66–7.57 (m, 1H), 7.175 (t,  $J = 12$  Hz, 1H), 7.09 (d,  $J = 8$  Hz, 2H), 6.28 (t,  $J = 16$  Hz, 2H), 5.765 (t,  $J = 12$  Hz, 1H), 2.93 (s, 6H), 1.57 (s, 9H), 1.53 (s, 9H);  $^{13}\text{C}$  NMR (101 MHz,  $\text{CD}_2\text{Cl}_2$ ,  $\delta$ ): 149.80, 148.79, 129.09, 127.26, 125.56, 123.27, 37.70, 37.45, 30.59, 30.53, 19.18;  $^{31}\text{P}$  NMR (161.9 MHz,  $\text{CD}_2\text{Cl}_2$ ,  $\delta$ ): 60.08;  $^{19}\text{F}$  NMR (376 MHz,  $\text{CD}_2\text{Cl}_2$ ,  $\delta$ ): -113.96, -118.08, -121.19, -126.36, -130.49, -134.65. HRMS (ESI)  $m/z$ : Calcd for  $\text{C}_{34}\text{C}_{39}\text{AuN}_2\text{P}^+ [\text{M} - \text{SbF}_6^-]$ , 703.2517. Found  $[\text{M} - \text{SbF}_6^-]$ , 703.2496  $\Delta = 0.0021$ . Mass error (ppm): -2.9861.

**Synthesis of AuTri-Phos 1d.** Prepared as described in the general procedure. AuCl<sub>3</sub>JohnPhos (100 mg, 0.1884 mmol), silver hexafluoroantimonate (71.2 mg, 0.2072 mmol), and 5-nitro-1,10-phenanthroline (42.5 mg, 0.1884 mmol). Yield: 145.4 mg, 81%.  $^1\text{H}$  NMR (400 MHz,  $\text{CD}_3\text{CN}$ ,  $\delta$ ): 9.26 (d,  $J = 8$  Hz, 1H), 9.08 (s, 1H) 9.015 (d,  $J = 2$  Hz, 1H), 8.98 (d,  $J = 4$  Hz, 1H), 8.95 (d,  $J = 4$  Hz, 1H), 8.21–8.12 (m, 3H), 7.65 (quint,  $J = 36$  Hz, 2H), 7.23 (s, 1H), 7.15 (d,  $J = 4$  Hz, 2H), 6.39 (s, 2H), 5.91 (s, 1H), 1.59 (s, 9H), 1.55 (s, 9H);  $^{13}\text{C}$  NMR (101 MHz,  $\text{CD}_3\text{CN}$ ,  $\delta$ ): 155.04, 152.52, 135.99, 134.44, 133.60,



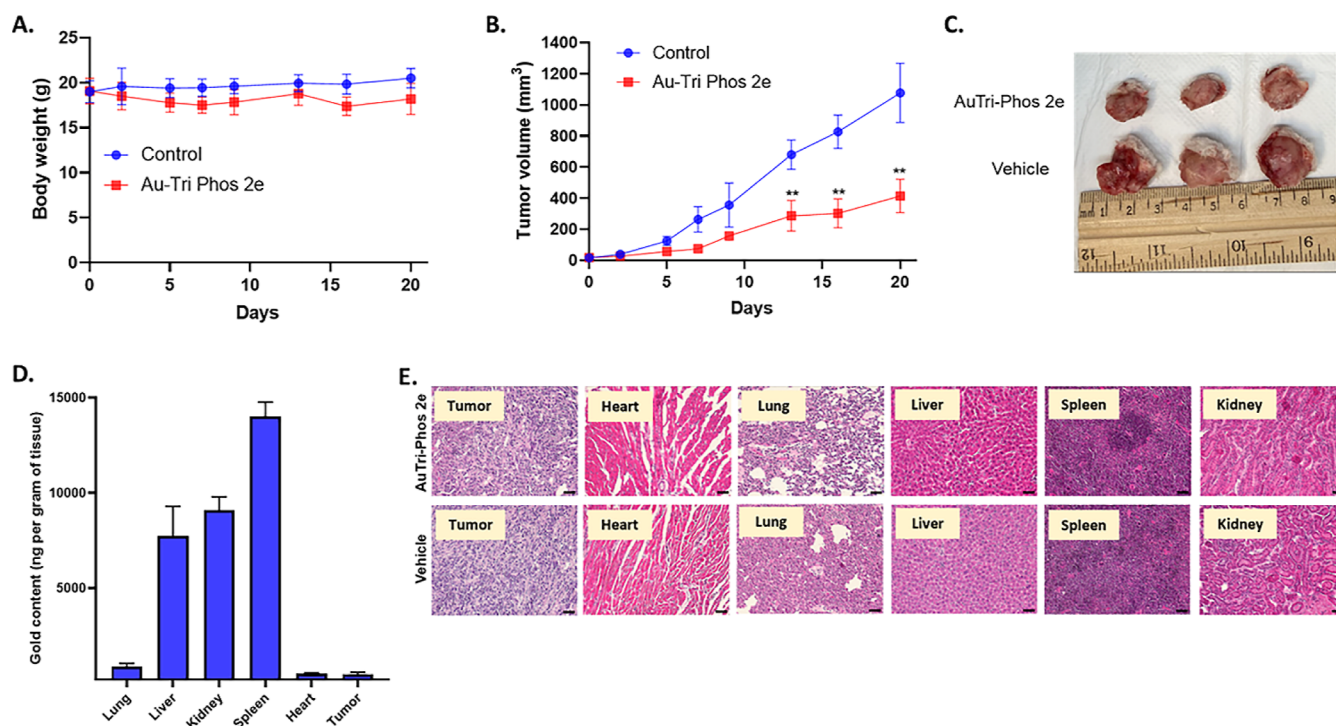


**Figure 6.** In vivo therapeutic potential of AuTri-Phos 2e. (A) Change in tumor volume following AuTri-Phos 2e administration over 20 days. Unpaired *t*-test, \**p* < 0.05 and \*\**p* < 0.01. (B) Representative images of tumor excised from the AuTri-Phos 2e and vehicle-treated mice. (C) Body weight of AuTri-Phos 2e and vehicle-treated mice. (D) Tissue biodistribution of gold in AuTri-Phos 2e treated mice determined by GF-AAS. (E) Hematoxylin and eosin (H&E) staining of harvested tissues and tumor. The scale bar represents 200  $\mu$ m.

129.85, 128.08, 126.96, 126.84, 126.79, 38.16, 37.90, 30.72, 30.65;  $^{31}\text{P}$  NMR (161.9 MHz,  $\text{CD}_3\text{CN}$ ,  $\delta$ ): 59.94;  $^{19}\text{F}$  NMR (376 MHz,  $\text{CD}_3\text{CN}$ ,  $\delta$ ): -111.13, -116.24, -121.41, -126.58, -131.73, -136.85. Anal. Calcd:  $\text{C}_{32}\text{H}_{34}\text{AuF}_6\text{N}_3\text{O}_2\text{PSb}$  C, 40.19%; H, 3.58%; N, 4.39%. Found:  $\text{C}_{32}\text{H}_{34}\text{AuF}_6\text{N}_3\text{O}_2\text{PSb} \cdot 1.05\text{H}_2\text{O}$  C, 39.72%; H, 3.62%; N, 3.98%.

**Synthesis of AuTri-Phos 1e.** Prepared as described in the general procedure. AuClJohnPhos (100 mg, 0.1884 mmol), silver hexafluoroantimonate (71.2 mg, 0.2072 mmol), and bathophenanthroline (62.6 mg, 0.1884 mmol). Yield: 97.7 mg, 49%.  $^1\text{H}$  NMR (400 MHz,  $\text{CD}_2\text{Cl}_2$ ,  $\delta$ ): 8.805 (d, *J* = 2 Hz, 2H), 8.10 (s, 2H), 8.06 (d, *J* = 8 Hz, 1H), 7.93 (d, *J* = 8 Hz, 2H), 7.64 (s, 8H), 7.61 (d, *J* = 8 Hz, 2H), 7.255 (t, *J* = 12 Hz, 1H), 7.20 (d, *J* = 8 Hz, 2H), 7.15 (d, *J* = 4 Hz, 2H), 6.51 (t, *J* = 16 Hz, 2H), 6.025 (t, *J* = 12 Hz, 1H), 1.62 (s, 9H), 1.58 (s, 9H);  $^{13}\text{C}$  NMR (101 MHz,  $\text{CD}_2\text{Cl}_2$ ,  $\delta$ ): 151.75, 149.78, 129.59, 129.06, 127.42, 125.15, 37.80, 30.64, 30.57;  $^{31}\text{P}$  NMR (161.9 MHz,  $\text{CD}_2\text{Cl}_2$ ,  $\delta$ ): 60.17;  $^{19}\text{F}$  NMR (376 MHz,  $\text{CD}_2\text{Cl}_2$ ,  $\delta$ ): -113.98, -118.16, -122.24, -126.49, -130.52, -134.67. Anal. Calcd:  $\text{C}_{44}\text{H}_{43}\text{AuF}_6\text{N}_2\text{PSb}$  C, 49.69%; H, 4.08%; N, 2.63%. Found:  $\text{C}_{44}\text{H}_{43}\text{AuF}_6\text{N}_2\text{PSb} \cdot 1.75\text{H}_2\text{O}$  C, 47.90%; H, 3.92%; N, 2.48%.

**Synthesis of AuTri-Phos 1f.** Prepared as described in the general procedure. AuClJohnPhos (100 mg, 0.1884 mmol), silver hexafluoroantimonate (71.2 mg, 0.2072 mmol), and dipyrrophenazine (53.2 mg, 0.1884 mmol). Yield: 111.6 mg, 58.5%.  $^1\text{H}$  NMR (400 MHz,  $\text{CD}_3\text{CN}$ ,  $\delta$ ): 9.84 (d, *J* = 8 Hz, 2H), 8.915 (d, *J* = 4 Hz, 2H), 8.46 (q, *J* = 8 Hz, 2H), 8.19–8.13 (m, 5H), 8.655 (dt, *J* = 16, 36 Hz, 2H), 7.215 (t, *J* = 12 Hz, 1H), 7.15 (d, *J* = 8 Hz, 2H), 6.44 (s, 2H), 5.99 (s, 1H), 1.63 (s, 9H), 1.59 (s, 9H);  $^{13}\text{C}$  NMR (101 MHz,  $\text{CD}_3\text{CN}$ ,  $\delta$ ): 151.19, 143.30, 140.60, 136.58, 134.48, 133.55, 132.69, 131.47, 130.13, 129.80, 128.11, 127.02, 38.16, 37.90, 30.78;  $^{31}\text{P}$  NMR (161.9 MHz,  $\text{CD}_3\text{CN}$ ,  $\delta$ ): 60.31;  $^{19}\text{F}$  NMR (376 MHz,  $\text{CD}_3\text{CN}$ ,  $\delta$ ): -111.16, -116.31, -121.43, -126.59, -131.73, -136.86.

**Synthesis of AuTri-Phos 2a.** Prepared as described in the general procedure. AuClCPhos (50 mg, 0.0746 mmol), silver hexafluoroantimonate (28.2 mg, 0.0821 mmol), and 1,10-phenanthroline (13.5 mg, 0.0746 mmol). Yield: 32.3 mg, 41%.  $^1\text{H}$  NMR (400 MHz,  $\text{CD}_3\text{CN}$ ,  $\delta$ ): 8.88 (s, 2H), 8.73 (dd, *J* = 4, 12 Hz, 2H), 8.34 (d, *J* = 8

Hz, 1H), 8.185 (d, *J* = 12 Hz, 1H), 8.015 (t, *J* = 12 Hz, 1H), 7.94–7.87 (m, 2H), 7.325 (quint, *J* = 12 Hz, 1H), 5.86 (s, 2H), 2.635 (q, *J* = 36 Hz, 2H), 2.31 (br, 2H), 2.27 (s, 12H), 2.15 (s, 1H), 2.04 (br, 2H), 1.775 (d, *J* = 12 Hz, 2H), 1.67–1.31 (m, 13H);  $^{13}\text{C}$  NMR (101 MHz,  $\text{CD}_3\text{CN}$ ,  $\delta$ ): 151.90, 143.10, 139.88, 135.94, 131.37, 130.69, 127.99, 125.45, 43.86, 36.99, 36.66, 32.81, 30.17, 27.43, 27.27, 27.09, 26.96, 26.26;  $^{31}\text{P}$  NMR (161.9 MHz,  $\text{CD}_3\text{CN}$ ,  $\delta$ ): 37.44;  $^{19}\text{F}$  NMR (376 MHz,  $\text{CD}_3\text{CN}$ ,  $\delta$ ): -111.13, -116.27, -121.42, -126.54, -131.77, -136.55. Anal. Calcd:  $\text{C}_{40}\text{H}_{49}\text{AuF}_6\text{N}_4\text{PSb}$  C, 45.78%; H, 4.71%; N, 5.34%. Found:  $\text{C}_{40}\text{H}_{49}\text{AuF}_6\text{N}_4\text{PSb} \cdot 1.05\text{H}_2\text{O}$  C, 45.67%; H, 4.65%; N, 5.25%.

**Synthesis of AuTri-Phos 2b.** Prepared as described in the general procedure. AuClCPhos (100 mg, 0.1492 mmol), silver hexafluoroantimonate (56.4 mg, 0.1642 mmol), and 4-methyl-1,10-phenanthroline (29 mg, 0.1492 mmol). Yield: 100.8 mg, 64%.  $^1\text{H}$  NMR (400 MHz,  $\text{CD}_3\text{CN}$ ,  $\delta$ ): 8.90 (s, 2H), 8.695 (dd, *J* = 4, 12 Hz, 2H), 8.34 (d, *J* = 8 Hz, 1H), 8.185 (d, *J* = 12 Hz, 1H), 8.00 (t, *J* = 8 Hz, 1H), 7.94–7.87 (m, 1H), 7.57 (quint, *J* = 32 Hz, 2H), 7.315 (t, *J* = 12 Hz, 1H), 5.83 (s, 2H), 5.78 (s, 1H), 2.95 (s, 3H), 2.635 (q, *J* = 36 Hz, 2H), 2.34 (d, *J* = 16 Hz, 2H), 2.22 (s, 12H), 1.775 (d, *J* = 12 Hz, 3H), 1.70–1.30 (m, 15H);  $^{13}\text{C}$  NMR (101 MHz,  $\text{CD}_3\text{CN}$ ,  $\delta$ ): 153.17, 151.59, 135.85, 127.54, 126.11, 125.32, 124.21, 112.52, 43.84, 37.04, 36.70, 32.83, 30.21, 27.44, 27.30, 27.11, 26.98, 26.30, 19.21;  $^{31}\text{P}$  NMR (161.9 MHz,  $\text{CD}_3\text{CN}$ ,  $\delta$ ): 37.59;  $^{19}\text{F}$  NMR (376 MHz,  $\text{CD}_3\text{CN}$ ,  $\delta$ ): -111.08, -116.18, -121.37, -126.51, -131.67, -136.81. Anal. Calcd:  $\text{C}_{41}\text{H}_{51}\text{AuF}_6\text{N}_4\text{PSb}$  C, 46.30%; H, 4.83%; N, 5.27%. Found:  $\text{C}_{41}\text{H}_{51}\text{AuF}_6\text{N}_4\text{PSb} \cdot 0.80\text{H}_2\text{O}$  C, 47.00%; H 5.04%; N, 5.17%.

**Synthesis of AuTri-Phos 2c.** Prepared as described in the general procedure. AuClCPhos (100 mg, 0.1492 mmol), silver hexafluoroantimonate (56.4 mg, 0.1642 mmol), and 4,7-dimethyl-1,10-phenanthroline (31.1 mg, 0.1492 mmol). Yield: 97.1 mg, 60%.  $^1\text{H}$  NMR (400 MHz,  $\text{CD}_3\text{CN}$ ,  $\delta$ ): 8.70 (s, 2H), 8.34 (s, 2H), 7.91 (s, 1H), 7.85 (d, *J* = 8 Hz, 1H), 7.61–7.55 (m, 3H), 7.32 (s, 1H), 5.81 (s, 2H), 5.75 (s, 1H), 2.94 (s, 6H), 2.61 (d, *J* = 8 Hz, 3H), 2.27 (s, 12H), 1.93 (s, 4H), 1.765 (d, *J* = 12 Hz, 2H), 1.66–1.30 (m, 13H);  $^{13}\text{C}$  NMR (101 MHz,  $\text{CD}_3\text{CN}$ ,  $\delta$ ): 151.27, 149.73, 135.83, 125.98,



123.80, 43.88, 32.81, 30.23, 27.29, 26.29, 19.11;  $^{31}\text{P}$  NMR (161.9 MHz,  $\text{CD}_3\text{CN}$ ,  $\delta$ ): 37.66;  $^{19}\text{F}$  NMR (376 MHz,  $\text{CD}_3\text{CN}$ ,  $\delta$ ): -111.13, -116.27, -121.41, -126.56, -131.33, -136.84. Anal. Calcd:  $\text{C}_{42}\text{H}_{53}\text{AuF}_6\text{N}_4\text{PSb}$  C, 46.81%; H, 4.96%; N, 5.20%. Found:  $\text{C}_{42}\text{H}_{53}\text{AuF}_6\text{N}_4\text{PSb} \cdot 1.95\text{H}_2\text{O}$  C, 45.14%; H, 4.82%; N, 4.79%. HRMS (ESI)  $m/z$ : calcd for  $\text{C}_{42}\text{C}_{53}\text{AuN}_4\text{P}^+ [\text{M} - \text{SbF}_6^-]$ , 841.3669. Found  $[\text{M} - \text{SbF}_6^-]$ , 841.3660  $\Delta = 0.0009$ . Mass error (ppm): -1.0697.

**Synthesis of AuTri-Phos 2d.** Prepared as described in the general procedure. AuClCPhos (50 mg, 0.0746 mmol), silver hexafluoroantimonate (28.2 mg, 0.0821 mmol), and 5-nitro-1,10-phenanthroline (16.8 mg, 0.0746 mmol). Yield: 40 mg, 49%.  $^1\text{H}$  NMR (400 MHz,  $\text{CD}_3\text{CN}$ ,  $\delta$ ): 9.29 (d,  $J = 8$  Hz, 1H), 8.95 (s, 1H), 8.93 (d,  $J = 8$  Hz, 1H), 8.89 (d,  $J = 8$  Hz, 1H), 8.85 (d,  $J = 8$  Hz, 1H), 8.155 (quint,  $J = 20$  Hz, 2H), 7.78 (t,  $J = 16$  Hz, 1H), 7.565 (q,  $J = 20$  Hz, 3H), 7.365 (t,  $J = 12$  Hz, 1H), 6.89 (d,  $J = 8$  Hz, 1H), 5.96 (s, 3H), 2.565 (q,  $J = 36$  Hz, 2H), 2.41 (s, 2H), 2.38 (s, 4H), 2.31 (s, 12H), 2.04–1.78 (m, 12H);  $^{13}\text{C}$  NMR (101 MHz,  $\text{CD}_2\text{Cl}_2$ ,  $\delta$ ): 154.32, 152.98, 151.70, 144.58, 143.88, 142.83, 141.62, 135.76, 135.69, 135.48, 132.75, 131.25, 127.93, 127.21, 127.15, 126.70, 126.13, 122.65, 111.96, 43.65, 36.90, 36.64, 32.75, 31.62, 29.82, 29.08, 27.28, 27.16, 26.91, 26.81, 25.95, 22.69, 18.53, 13.91, 11.22;  $^{31}\text{P}$  NMR (161.9 MHz,  $\text{CD}_3\text{CN}$ ,  $\delta$ ): 39.14;  $^{19}\text{F}$  NMR (376 MHz,  $\text{CD}_2\text{Cl}_2$ ,  $\delta$ ): -113.61, -117.33, -121.35, -126.19, -130.80, -134.52. Anal. Calcd:  $\text{C}_{40}\text{H}_{48}\text{AuF}_6\text{N}_5\text{O}_2\text{PSb}$  C, 43.89%; H, 4.42%; N, 6.40%. Found:  $\text{C}_{40}\text{H}_{48}\text{AuF}_6\text{N}_5\text{O}_2\text{PSb} \cdot 1.6\text{C}_4\text{H}_{10}\text{O} \cdot 1\text{H}_2\text{O}$  C, 45.04%; H, 5.15%; N, 5.44%.

**Synthesis of AuTri-Phos 2e.** Prepared as described in the general procedure. AuClCPhos (100 mg, 0.1492 mmol), silver hexafluoroantimonate (56.4 mg, 0.1642 mmol), and bathophenanthroline (49.6 mg, 0.1492 mmol). Yield: 141.8 mg, 79%.  $^1\text{H}$  NMR (400 MHz,  $\text{CD}_3\text{CN}$ ,  $\delta$ ): 8.92 (s, 1H), 8.07 (s, 2H), 7.92 (t,  $J = 16$  Hz, 3H), 7.66 (s, 12H), 7.56 (t,  $J = 16$  Hz, 2H), 7.31 (s, 1H), 5.91 (s, 2H), 2.64 (q,  $J = 32$  Hz, 2H), 2.42 (s, 1H), 2.35 (d,  $J = 16$  Hz, 3H), 2.28 (s, 12H), 2.05 (s, 2H), 1.79–1.33 (m, 12H);  $^{13}\text{C}$  NMR (101 MHz,  $\text{CD}_2\text{Cl}_2$ ,  $\delta$ ): 151.10, 150.55, 143.56, 136.75, 129.70, 129.41, 129.03, 127.46, 125.21, 124.97, 67.25, 57.46, 36.07;  $^{31}\text{P}$  NMR (161.9 MHz,  $\text{CD}_3\text{CN}$ ,  $\delta$ ): 37.87;  $^{19}\text{F}$  NMR (376 MHz,  $\text{CD}_3\text{CN}$ ,  $\delta$ ): -111.21, -116.34, -121.49, -126.62, -131.78, -136.87. Anal. Calcd:  $\text{C}_{52}\text{H}_{57}\text{AuF}_6\text{N}_4\text{PSb}$  C, 51.97%; H, 4.78%; N, 4.66%. Found:  $\text{C}_{52}\text{H}_{57}\text{AuF}_6\text{N}_4\text{PSb} \cdot 0.25\text{C}_6\text{H}_{14}$  C, 52.82%; H, 4.60%; N, 4.76%. HRMS (ESI)  $m/z$ : Calcd for  $\text{C}_{52}\text{C}_{57}\text{AuN}_4\text{P}^+ [\text{M} - \text{SbF}_6^-]$ , 965.3955; found  $[\text{M} - \text{SbF}_6^-]$ , 965.3987  $\Delta = 0.0032$ . Mass error (ppm): 3.3147.

**Synthesis of AuTri-Phos 3b.** Prepared as described in the general procedure. AuClSPhos (72.1 mg, 0.1121 mmol), silver hexafluoroantimonate (42.4 mg, 0.1234 mmol), and 4-methyl-1,10-phenanthroline (21.8 mg, 0.1121 mmol). Yield: 88 mg, 76%.  $^1\text{H}$  NMR (400 MHz,  $\text{CD}_3\text{CN}$ ,  $\delta$ ): 8.89 (s, 1H), 8.70 (s, 2H), 8.32 (s, 1H), 8.16 (s, 1H), 8.03 (s, 1H), 7.89 (s, 1H), 7.845 (t,  $J = 12$  Hz, 1H), 7.545 (t,  $J = 12$  Hz, 2H), 6.985 (t,  $J = 12$  Hz, 1H), 5.76 (t,  $J = 16$  Hz, 1H), 5.48 (d,  $J = 8$  Hz, 2H), 3.39 (s, 6H), 2.93 (s, 3H), 2.44 (d,  $J = 8$  Hz, 2H), 2.21 (s, 2H), 1.89 (s, 4H), 1.78 (s, 4H), 1.52–1.40 (m, 10H);  $^{13}\text{C}$  NMR (101 MHz,  $\text{CD}_2\text{Cl}_2$ ,  $\delta$ ): 157.55, 151.05, 150.26, 149.57, 142.76, 142.33, 139.01, 138.29, 133.29, 133.22, 131.99, 131.06, 131.04, 129.81, 129.71, 128.36, 127.64, 127.58, 127.30, 125.80, 124.84, 123.77, 119.45, 102.88, 55.28, 37.03, 31.33, 29.98, 26.77, 26.67, 26.64, 26.52, 26.18, 26.17, 19.44;  $^{31}\text{P}$  NMR (161.9 MHz,  $\text{CD}_3\text{CN}$ ,  $\delta$ ): 38.00;  $^{19}\text{F}$  NMR (376 MHz,  $\text{CD}_2\text{Cl}_2$ ,  $\delta$ ): -111.49, -121.87, -127.02, -137.37. Anal. Calcd  $\text{C}_{39}\text{H}_{45}\text{AuF}_6\text{N}_2\text{O}_2\text{PSb}$  C, 45.15%; H, 4.37%; N, 2.70%. Found:  $\text{C}_{39}\text{H}_{45}\text{AuF}_6\text{N}_2\text{O}_2\text{PSb}$  C, 45.23%; H, 4.31%; N, 3.05%.

**Synthesis of AuTri-Phos 3d.** Prepared as described in the general procedure. AuClSPhos (100 mg, 0.1543 mmol), silver hexafluoroantimonate (58 mg, 0.1698 mmol), and 5-nitro-1,10-phenanthroline (34.7 mg, 0.1543 mmol). Yield: 125.2 mg, 76%.  $^1\text{H}$  NMR (400 MHz,  $\text{CD}_3\text{CN}$ ,  $\delta$ ): 9.82 (d,  $J = 8$  Hz, 2H), 8.895 (d,  $J = 4$  Hz, 2H), 8.45 (dd,  $J = 4, 8$  Hz, 2H), 8.195 (dd,  $J = 4, 12$  Hz, 2H), 8.13 (dd,  $J = 4, 12$  Hz, 2H), 7.86 (s, 1H), 7.55 (s, 2H), 7.00 (s, 1H), 5.69 (s, 1H), 3.44 (s, 6H), 2.46 (s, 2H), 2.24 (s, 2H), 1.79 (s, 5H), 1.53 (s, 5H), 1.42 (s, 7H);  $^{13}\text{C}$  NMR (101 MHz,  $\text{CD}_3\text{CN}$ ,  $\delta$ ): 158.02, 152.55, 126.98,

55.58, 26.75, 26.35;  $^{31}\text{P}$  NMR (161.9 MHz,  $\text{CD}_3\text{CN}$ ,  $\delta$ ): 38.37;  $^{19}\text{F}$  NMR (376 MHz,  $\text{CD}_3\text{CN}$ ,  $\delta$ ): -111.14, -116.23, -121.45, -126.55, -136.91. Anal. Calcd  $\text{C}_{38}\text{H}_{42}\text{AuF}_6\text{N}_3\text{O}_4\text{PSb}$  C, 42.72%; H, 3.96%; N, 3.93%. Found:  $\text{C}_{38}\text{H}_{42}\text{AuF}_6\text{N}_3\text{O}_4\text{PSb} \cdot 0.45\text{C}_6\text{H}_{14}$  C, 43.99%; H, 4.31%; N, 3.52%.

**Synthesis of AuTri-Phos 3f.** Prepared as described in the general procedure. AuClSPhos (50 mg, 0.0705 mmol), silver hexafluoroantimonate (27 mg, 0.0755 mmol), and dipyrindophenazine (20 mg, 0.0705 mmol). Yield: 33.1 mg, 42%.  $^1\text{H}$  NMR (400 MHz,  $\text{CD}_3\text{CN}$ ,  $\delta$ ): 9.82 (d,  $J = 8$  Hz, 2H), 8.9 (s, 2H), 8.445 (dd,  $J = 4, 12$  Hz, 2H), 8.195 (dd,  $J = 4, 12$  Hz, 2H), 8.125 (dd,  $J = 4, 12$  Hz, 2H), 7.86 (t,  $J = 16$  Hz, 1H), 7.55 (s, 2H), 6.99 (s, 1H), 3.41 (s, 6H), 2.49 (s, 2H), 2.26 (s, 2H), 1.79 (s, 4H), 1.54 (s, 4H), 1.44 (d,  $J = 8$  Hz, 6H);  $^{13}\text{C}$  NMR (101 MHz,  $\text{CD}_2\text{Cl}_2$ ,  $\delta$ ): 157.69, 152.06, 144.55, 142.12, 139.58, 136.78, 133.33, 133.26, 132.30, 131.99, 131.18, 129.78, 128.51, 127.78, 127.69, 127.34, 126.32, 103.01, 55.40, 37.01, 36.73, 31.38, 30.10, 26.78, 26.68, 26.65, 26.54, 26.19, 26.17;  $^{31}\text{P}$  NMR (161.9 MHz,  $\text{CD}_2\text{Cl}_2$ ,  $\delta$ ): 38.51;  $^{19}\text{F}$  NMR (376 MHz,  $\text{CD}_2\text{Cl}_2$ ,  $\delta$ ): -113.93, -118.14, -122.19, -126.29, -130.57, -134.71.

**Physical and Chemical Characterization. X-ray Crystallography.** Crystals were grown via two methods. Method 1: diethyl ether was slowly diffused into concentrated solutions of AuTri-Phos 1c and 2c in DCM at room temperature. Method 2: saturated solutions of AuTri-Phos 1d–1f in acetonitrile were heated to 70 °C and then cooled to 4 °C. All crystals were mounted using polyisobutene oil on the end of a glass fiber, which was mounted to a copper pin. It was placed directly in the cold gas stream of a liquid nitrogen cryostat.<sup>92</sup> A Bruker D8 Venture diffractometer with multilayer focused Mo  $K\alpha$  X-rays ( $\lambda = 0.71073$  Å) was used to collect diffraction. Raw data were integrated, scaled, merged, and corrected for Lorentz-polarization effects using APEX3 package.<sup>93</sup> Space group determination and refinement were carried out with SHELXT and SHELXL.<sup>94,95</sup> All non-hydrogen atoms were refined with anisotropic displacement parameters. Hydrogen atoms were placed at calculated positions and refined using a riding model with their isotropic displacement parameters (Uiso) set to either 1.2Uiso or 1.5Uiso of the atom to which they were attached. Ellipsoid plots were drawn using SHELXTL-XP. The structures, deposited in the Cambridge Structural Database, were checked for missed symmetry, twinning, and overall quality with PLATON, an R-tensor, and finally validated using CheckCIF.<sup>96,97</sup>

**Photochemical Characterization (UV–Vis).** Stock solutions (1 mM) of AuTri-Phos 1a–3f were made in DMSO and diluted down to 50  $\mu\text{M}$ . All absorption spectra were recorded on a Shimadzu UV-1280 model instrument. Prior to each run, the instrument was blanked with the DI  $\text{H}_2\text{O}$ .

**Reactivity of AuTri-Phos 2e with L-GSH.** Stock solution of AuTri-Phos 2e (1 mM) was prepared in DMSO. The stock solution was then diluted using DMEM to a concentration of 100  $\mu\text{M}$ . 1 mM stock of L-GSH was also prepared separately in DMEM. Equal volume of L-GSH and 2e were combined, bringing the final molar ratio of 1:10 of 2e and L-GSH. The solution mixture was transferred to a quartz cuvette and initial UV–vis spectra was recorded using a Shimadzu UV–vis spectrometer for a 1 h time point reading. The mixture was then incubated at 37 °C for 25 h with readings taken at time points 2, 7, 13, and 25 h using the Shimadzu UV–vis spectrometer.

**Reactivity of AuTri-Phos 2e with Bovine Serum Albumin.** A 1 mM stock solution of 2e in DMSO was prepared and diluted down to 100  $\mu\text{M}$ . Separately, a 2.5 M stock solution of BSA in PBS was prepared and diluted down to 1 mM. Equal volumes of the two solutions were combined to make a 50  $\mu\text{M}$  and 500  $\mu\text{M}$  of 2e and BSA, respectively, and absorbance spectra were recorded at 1, 2, 7, 13, and 25 h.

**In Vitro Biological Characterization. Cell Culture.** Cells used were patient derived and grown in a humidified incubator at 37 °C with 5–10%  $\text{CO}_2$ . MDA-MB-468 and MDA-MB-231 cells were grown in DMEM supplemented with 10% FBS, 1% amphotericin, and 1% penicillin/streptomycin. All supplements along with PBS and trypsin–EDTA were purchased from Corning Inc. and used as is.

**Cell Viability of AuTri-Phos Complexes.** The cell viability of all 14 complexes were evaluated in the MDA-MB-468 and MDA-MB-231 cell lines. Cells were grown to confluency and trypsin was added to detach and harvest cells. The cells were washed with 2 mL of PBS and suspended in 10 mL of the DMEM. The cells were centrifuged at 2000 rpm for 10 min and the pellet washed carefully with 1 mL of PBS then suspended in 5 mL of the DMEM. The cells were plated at a density of 2000 cells/well in a 96-well clear bottom plate and allowed to adhere overnight at 37 °C with 5–10% CO<sub>2</sub>. The compounds were prepared as stock in DMSO and used fresh. The compounds were added at seven concentrations (<1% DMSO) with a 3× serial dilution starting at 50 μM for the highest concentration and incubated at 37 °C for 72 h with 5–10% CO<sub>2</sub>. The medium was removed and a solution of MTT (100 μL, prepared by dissolving MTT at 5 mg/mL and diluting by 10× with DMEM) was added to each well and incubated for 4 h at 37 °C with 5–10% CO<sub>2</sub>. The dye was removed from each well and 100 μL of DMSO was added to induce cell lysis. The plates were read using a Genios plate reader (λ = 570 nm). The experiment was performed in triplicate and data are plotted as the mean ± s.e.m. (n = 3).

**Solution Stability of AuTri-Phos Complexes.** DMEM was warmed to 37 °C prior to use. All absorption spectra were recorded on a Shimadzu UV-1280 model instrument. Prior to each run, the instrument was blanked with the corresponding buffer/solvent. The solutions were incubated at 37 °C until used for absorption measurement. AuTri-Phos complexes were prepared as a 1 mM stock in DMSO and diluted down to 50 μM with the corresponding medium. No precipitation was observed. The absorption spectra were recorded at 1, 2, 7, 13, and 25 h.

**Immunoblotting.** Equal numbers of MDA-MB-468 cells were seeded and treated with AuTri-Phos **2e** for the indicated time points. Whole cell lysates were prepared using RIPA buffer, 1× protease inhibitor cocktail (Sigma), and 1× phosphatase inhibitor cocktails I and II (Sigma) and loaded by equal protein for SDS–PAGE. Cell lysates containing equal amounts of protein were separated on a 4–20% SDS–polyacrylamide gel. Post separation, proteins were transferred to a nitrocellulose membrane and nonspecific binding sites were blocked by treating with bovine serum albumin (BSA) in PBST for 1 h. The membranes were incubated overnight with the primary antibodies directed against listed proteins. Appropriate secondary antibodies were used accordingly. The membranes were placed in pierce enhanced chemiluminescence substrate and visualized with Bio-Rad imager. All antibodies used for this study were purchased from cell signaling technology.

**Mitochondrial ROS.** MDA-MB-468 cells were plated in a six-well plate at 500,000 cells per well and allowed to adhere overnight. Cells were treated with AuTri-Phos **2e** for short period of 2 h at concentrations of 2 μM and 5 μM. After incubation time with test compound, cells were trypsinized and centrifuged to form pellets. Pellets were washed with PBS and resuspended in Mitosox dye solution (200 μL). This was transferred into FACS tube and incubated for 20 min followed by flow cytometry analysis.

**Bioenergetics Analysis with Seahorse XF96.** Bioenergetics was analyzed via two methods, pneumatic injection and pretreatment. BT333 cells were seeded at 30,000 cells/well for the Seahorse XF96 experiments. The cells were seeded a day prior to the experiment in a 100 μL volume per well and incubated overnight at 37 °C. AuTri-Phos **2e** was prepared as a 1 mM stock in DMSO and phenol red free DMEM and diluted to working concentration with Seahorse XF96 assay buffer. The pneumatic injection assay was performed with the final injection concentrations of 2, 5, and 10 μM (<1% DMSO). This was followed by injection of oligomycin (1.5 μM), FCCP (0.6 μM) and rotenone/antimycin A (0.5 μM). The metabolic parameters are calculated based on readings from a minimum of 3 wells.

**Whole Cell Uptake Analysis.** MDA-MB-468 cells were seeded at a density of 1 × 10<sup>6</sup> in a 6-well plate and allowed to adhere overnight at 37 °C. Cells were treated with compound for 18 h, collected via trypsinization, and centrifuged at 2000 rpm for 5 min to form a pellet. The pellet was suspended in 1 mL of DMEM, transferred to 1.5 mL Eppendorf tube, and centrifuged at 2000 rpm for 5 min. The media

was removed, and pellets were resuspended and washed in PBS (1 mL × 2) and stored at –20 °C until further analysis. Prior to analysis, pellets were suspended in 200 μL of 70% HNO<sub>3</sub> digested for 4 h, allowed to cool to room temperature, and diluted appropriately before being analyzed on GF-AAS. Cellular gold concentration was expressed as pmol of Au per million cells.

**Apoptosis Analysis.** MDA-MB-468 cells were seeded at a density of 5 × 10<sup>5</sup> cells/well in a 6-well clear bottom plate with a final media volume of 2 mL. The cells were allowed to adhere overnight at 37 °C. A stock of AuTri-Phos **2e** was prepared fresh in DMSO and added to the desired well at a concentration of 2 μM with a final volume of 2.5 mL and incubated for 4 h at 37 °C. The media was removed, and the wells were washed with 5 mL of PBS. The cells were trypsinized (1 mL), 5 mL of DMEM was added to each well, and the total volume was collected and centrifuged to pellet the cells. The cells were resuspended in 2 mL of fresh media, counted, and reconstituted to a concentration of 1 × 10<sup>5</sup> cells/mL. The cells were centrifuged again, and the pellets were suspended in 500 μL of Annexin binding buffer. To each sample was added 5 μL of Annexin V-FITC and 5 μL PI and incubated in the dark at room temperature for 5 min. The samples were then subjected to FACS analysis. Graphs are representative of three technical replicates.

**Animal Experiment. In Vivo Experiment.** Five-week-old female BALB/c mice were purchased from Jackson Laboratories and quarantined for a period of 1 week before inoculation with 1,000,000 4T1 cells subcutaneously on their right flanks. After 3 days of implantation, the mice were systemically treated with 10 mg/kg AuTri-Phos **2e** via intraperitoneal administration. AuTri-Phos **2e** was formulated in DMSO (1%), Kolliphor (10%), and PBS (89%) and delivered at 100 μL. The control group was treated with a PBS solution containing 1% DMSO and 10% Kolliphor. The injection of AuTri-Phos **2e** was performed three times a week for 2 weeks. Tumor size and body weight measurements were performed 3 days a week, and mice were euthanized 15 days later. All mice were maintained in a pathogen-free environment under the care of DLAR of University of Kentucky. Our study was performed in compliance with the NIH guidelines (NIH publication no. 85-23 Rev. 1985) for the care and use of laboratory animals and all experimental procedures were monitored and approved by the Institutional Animal Care and Use Committee (IACUC# 2019-3183) of University of Kentucky (USA).

**Hematoxylin and Eosin Staining.** The mice used in the in vivo comparative experiment of AuTri-Phos **2e** were sacrificed at day 14 post tumor cell (4T1) injection. Freshly prepared paraformaldehyde (4% in PBS) was used to fix harvested mice organs (heart, lung, liver, kidney, spleen, and tumor) for 24 h before being processed for paraffin sectioning. The organ sections of 5 μm were stained with H&E staining and used for histological examination of the organs and tumor. A total of 5 sections per tissue (spanning the full depth of the organ) were examined and photographed using a Nikon Eclipse 55i microscope.

**Tissue Biodistribution.** Tissues obtained from the in vivo studies were used for tissue biodistribution. The tissues were boiled for 5 h at 60 °C with 70% HNO<sub>3</sub> (0.5 mL) and then boiled again at 60 °C for 10 min by adding 35% hydrogen peroxide (0.5 mL). The solution turned yellow and was diluted as needed to measure the gold content using a GF-AAS. Before measuring all samples, the standard solution curves were measured.

## ■ ASSOCIATED CONTENT

### Supporting Information

The Supporting Information is available free of charge at <https://pubs.acs.org/doi/10.1021/acs.jmedchem.5c00608>.

Crystal data and structure refinement for AuTri-Phos class of compounds. CCDC numbers for 2368622–2368626. <sup>1</sup>H, <sup>13</sup>C, <sup>31</sup>P spectra, HRMS, and UV–vis spectra for AuTri-Phos compounds and solution stability. Standard curve for whole cell uptake and



cropped/uncropped Western blot images. Atomic coordinates of crystal structures will be released (PDF) AuTri-Phos **1a–1f**, **2a–2e**, and **3b**, **3d**, **3f** (CSV)

## AUTHOR INFORMATION

### Corresponding Author

**Samuel G. Awuah** – Department of Chemistry, University of Kentucky, Lexington, Kentucky 40506, United States; Center for Pharmaceutical Research and Innovation, Department of Pharmaceutical Sciences, College of Pharmacy and Markey Cancer Center, University of Kentucky, Lexington, Kentucky 40536, United States; Center for Bioelectronics and Nanomedicine, University of Kentucky, Lexington, Kentucky 40506, United States; [orcid.org/0000-0003-4947-7283](https://orcid.org/0000-0003-4947-7283); Email: [awuah@uky.edu](mailto:awuah@uky.edu)

### Authors

**Charles E. Greif** – Department of Chemistry, University of Kentucky, Lexington, Kentucky 40506, United States

**Owamagbe N. Orobator** – Department of Chemistry, University of Kentucky, Lexington, Kentucky 40506, United States

**Chibuzor Olelewe** – Department of Chemistry, University of Kentucky, Lexington, Kentucky 40506, United States

**Sean Parkin** – Department of Chemistry, University of Kentucky, Lexington, Kentucky 40506, United States

Complete contact information is available at:

<https://pubs.acs.org/10.1021/acs.jmedchem.5c00608>

### Author Contributions

Conceptualization, C.E.G. and S.G.A.; methodology, C.E.G.; synthesis and characterization, C.E.G.; X-ray crystallography, S.P.; Biological assays, C.E.G., O.N.O., and C.O.; in vivo studies, C.E.G.; seahorse assay and MMP studies C.E.G.; UV-vis spectrometry C.E.G.; in vivo biological studies, O.N.O. and C.O.; writing—original draft preparation, C.E.G. and S.G.A.; writing—review and editing, C.E.G. and S.G.A.; supervision, S.G.A.; funding acquisition, S.G.A.

### Funding

This work and S.G.A. was supported by grant R01CA258421-01 from the National Cancer Institute.

### Notes

The authors declare the following competing financial interest(s): S.G.A. has patents pending to University of Kentucky Research Foundation. S.G.A. serves on the advisory board and is Chief Executive Officer of Ayarissa Biosciences.

## ACKNOWLEDGMENTS

We are grateful for financial support from the National Institute of Health (NIH) P20GM130456 (S.G.A.). We would like to thank the following facilities at the University of Kentucky who provided support in completion of the experiments detailed in this manuscript. The UK NMR Center supported by NSF (CHE-997738) and the UK X-ray facility supported by the MRI program from NSF (CHE-1625732). For the flow cytometry experiments, we would like to thank UK Flow Cytometry and Immune Function core supported by the Office of the Vice President of Research, the Markey Cancer Center, and NCI Center Core Support Grant (P30 CA177558). We thank Dr. Chris Richard's lab for access and assistance with fluorescence microscopy.

## ABBREVIATIONS

BRCA, breast cancer gene; DCM, dichloromethane; DMEM, Dulbecco's modified Eagles medium; DMSO, dimethyl sulfoxide; DPPZ, dipyrrophenazine; FACS, fluorescence-assisted cell sorting; FBS, fetal bovine serum; FCCP, carbonyl cyanide-*p*-trifluoromethoxyphenylhydrazone; GF-AAS, graphite furnace atomic absorption spectroscopy; L-GHS, L-gultathione; NMR, nuclear magnetic resonance; PARP, poly(ADP-ribose) polymerase; PBS, phosphate buffer solution; PD-L1, programmed death ligand 1; SAR, structure activity relationship; SDS-PAGE, sodium dodecyl-sulfate polyacrylamide gel electrophoresis; TNBC, triple negative breast cancer

## REFERENCES

- (1) Eckstein, N. Platinum resistance in breast and ovarian cancer cell lines. *J. Exp. Clin. Cancer Res.* **2011**, *30* (1), 91.
- (2) Hill, D. P.; Harper, A.; Malcolm, J.; McAndrews, M. S.; Mockus, S. M.; Patterson, S. E.; Reynolds, T.; Baker, E. J.; Bult, C. J.; Chesler, E. J.; et al. Cisplatin-resistant triple-negative breast cancer subtypes: multiple mechanisms of resistance. *BMC Cancer* **2019**, *19* (1), 1039.
- (3) Cao, J.-J.; Zheng, Y.; Wu, X.-W.; Tan, C.-P.; Chen, M.-H.; Wu, N.; Ji, L.-N.; Mao, Z.-W. Anticancer Cyclometalated Iridium(III) Complexes with Planar Ligands: Mitochondrial DNA Damage and Metabolism Disturbance. *J. Med. Chem.* **2019**, *62* (7), 3311–3322.
- (4) Wang, F.-X.; Chen, M.-H.; Hu, X.-Y.; Ye, R.-R.; Tan, C.-P.; Ji, L.-N.; Mao, Z.-W. Ester-Modified Cyclometalated Iridium(III) Complexes as Mitochondria-Targeting Anticancer Agents. *Sci. Rep.* **2016**, *6* (1), 38954.
- (5) Olelewe, C.; Awuah, S. G. Mitochondria as a target of third row transition metal-based anticancer complexes. *Curr. Opin. Chem. Biol.* **2023**, *72*, 102235.
- (6) Bruijninx, P. C.; Sadler, P. J. Controlling Platinum, Ruthenium and Osmium Reactivity for Anticancer Drug Design. *Adv. Inorg. Chem.* **2009**, *61*, 1–62.
- (7) Zeng, L.; Gupta, P.; Chen, Y.; Wang, E.; Ji, L.; Chao, H.; Chen, Z.-S. The development of anticancer ruthenium(II) complexes: from single molecule compounds to nanomaterials. *Chem. Soc. Rev.* **2017**, *46* (19), 5771–5804.
- (8) Faller, J. W.; D'Alles, D. G. Planar Chirality in Tethered  $\eta^6\eta^1$ -(Phosphinophenylenearene-P)ruthenium(II) Complexes and Their Potential Use as Asymmetric Catalysts. *Organometallics* **2003**, *22* (13), 2749–2757.
- (9) Kostova, I. Ruthenium complexes as anticancer agents. *Curr. Med. Chem.* **2006**, *13* (9), 1085–1107.
- (10) Schindler, K.; Zobi, F. Anticancer and Antibiotic Ruthenium Tri- and Dicarboxyl Complexes: Current Research and Future Perspectives. *Molecules* **2022**, *27* (2), 539.
- (11) Greif, C. E.; Mertens, R. T.; Berger, G.; Parkin, S.; Awuah, S. G. An anti-glioblastoma gold(I)–NHC complex distorts mitochondrial morphology and bioenergetics to induce tumor growth inhibition. *RSC Chem. Biol.* **2023**, *4* (8), 592–599.
- (12) Roder, C.; Thomson, M. J. Auranofin: repurposing an old drug for a golden new age. *Drugs R&D* **2015**, *15* (1), 13–20.
- (13) Jellicoe, M. M.; Nichols, S. J.; Callus, B. A.; Baker, M. V.; Barnard, P. J.; Berners-Price, S. J.; Whelan, J.; Yeoh, G. C.; Filipovska, A. Bioenergetic differences selectively sensitize tumorigenic liver progenitor cells to a new gold(I) compound. *Carcinog* **2008**, *29* (6), 1124–1133.
- (14) Berners-Price, S. J.; Girard, G. R.; Hill, D. T.; Sutton, B. M.; Jarrett, P. S.; Faucette, L. F.; Johnson, R. K.; Mirabelli, C. K.; Sadler, P. J. Cytotoxicity and antitumor activity of some tetrahedral bis(diphosphino)gold(I) chelates. *J. Med. Chem.* **1990**, *33* (5), 1386–1392.
- (15) Ofori, S.; Gukathasan, S.; Awuah, S. G. Gold-Based Pharmacophore Inhibits Intracellular MYC Protein. *Chem. - Eur. J.* **2021**, *27* (12), 4168–4175.



- (16) Balfourier, A.; Kolosnjaj-Tabi, J.; Luciani, N.; Carn, F.; Gazeau, F. Gold-based therapy: From past to present. *Proc. Natl. Acad. Sci. U.S.A.* **2020**, *117* (37), 22639–22648.
- (17) Bertrand, B.; Citta, A.; Franken, I. L.; Picquet, M.; Folda, A.; Scalcon, V.; Rigobello, M. P.; Le Gendre, P.; Casini, A.; Bodio, E. Gold(I) NHC-based homo- and heterobimetallic complexes: synthesis, characterization and evaluation as potential anticancer agents. *J. Biol. Inorg. Chem.* **2015**, *20* (6), 1005–1020.
- (18) Rackham, O.; Nichols, S. J.; Leedman, P. J.; Berners-Price, S. J.; Filipovska, A. A gold(I) phosphine complex selectively induces apoptosis in breast cancer cells: implications for anticancer therapeutics targeted to mitochondria. *Biochem. Pharmacol.* **2007**, *74* (7), 992–1002.
- (19) Liu, J. J.; Galetti, P.; Farr, A.; Maharaj, L.; Samarasingha, H.; McGeachan, A. C.; Baguley, B. C.; Bowen, R. J.; Berners-Price, S. J.; McKeage, M. J. In vitro antitumor and hepatotoxicity profiles of Au(I) and Ag(I) bidentate pyridyl phosphine complexes and relationships to cellular uptake. *J. Inorg. Biochem.* **2008**, *102* (2), 303–310.
- (20) Zhang, J.; Zou, H.; Lei, J.; He, B.; He, X.; Sung, H. H. Y.; Kwok, R. T. K.; Lam, J. W. Y.; Zheng, L.; Tang, B. Z. Multifunctional Au(I)-based AIEgens: Manipulating Molecular Structures and Boosting Specific Cancer Cell Imaging and Theranostics. *Angew. Chem., Int. Ed. Engl.* **2020**, *59* (18), 7097–7105.
- (21) Hyun Kim, J.; Ofori, S.; Mertens, R. T.; Parkin, S.; Awuah, S. G. Water-Soluble Gold(III)–Metformin Complex Alters Mitochondrial Bioenergetics in Breast Cancer Cells. *ChemMedChem* **2021**, *16* (20), 3222–3230.
- (22) Man, X.; Li, W.; Zhu, M.; Li, S.; Xu, G.; Zhang, Z.; Liang, H.; Yang, F. Anticancer Tetranuclear Cu(I) Complex Catalyzes a Click Reaction to Synthesize a Chemotherapeutic Agent in situ to Achieve Targeted Dual-Agent Combination Therapy for Cancer. *Angew. Chem., Int. Ed. Engl.* **2024**, *63* (51), No. e202411846.
- (23) Li, W.; Li, T.; Pan, Y.; Li, S.; Xu, G.; Zhang, Z.; Liang, H.; Yang, F. Designing a Mitochondria-Targeted Theranostic Cyclometalated Iridium(III) Complex: Overcoming Cisplatin Resistance and Inhibiting Tumor Metastasis through Necroptosis and Immune Response. *J. Med. Chem.* **2024**, *67* (5), 3843–3859.
- (24) Man, X.; Li, S.; Xu, G.; Li, W.; Zhu, M.; Zhang, Z.; Liang, H.; Yang, F. Developing a Copper(II) Isopropyl 2-Pyridyl Ketone Thiosemicarbazone Compound Based on the IB Subdomain of Human Serum Albumin-Indomethacin Complex: Inhibiting Tumor Growth by Remodeling the Tumor Microenvironment. *J. Med. Chem.* **2024**, *67* (7), 5744–5757.
- (25) Jiang, M.; Li, W.; Liang, J.; Pang, M.; Li, S.; Xu, G.; Zhu, M.; Liang, H.; Zhang, Z.; Yang, F. Developing a Palladium(II) Agent to Overcome Multidrug Resistance and Metastasis of Liver Tumor by Targeted Multiacting on Tumor Cell, Inactivating Cancer-Associated Fibroblast and Activating Immune Response. *J. Med. Chem.* **2024**, *67* (18), 16296–16310.
- (26) Ho, C. M.; Zhang, J. L.; Zhou, C. Y.; Chan, O. Y.; Yan, J. J.; Zhang, F. Y.; Huang, J. S.; Che, C. M. A water-soluble ruthenium glycosylated porphyrin catalyst for carbenoid transfer reactions in aqueous media with applications in bioconjugation reactions. *J. Am. Chem. Soc.* **2010**, *132* (6), 1886–1894.
- (27) Vinogradova, E. V.; Zhang, C.; Spokoyny, A. M.; Pentelute, B. L.; Buchwald, S. L. Organometallic palladium reagents for cysteine bioconjugation. *Nature* **2015**, *526* (7575), 687–691.
- (28) On-Yee Chan, A.; Lui-Lui Tsai, J.; Kar-Yan Lo, V.; Li, G.-L.; Wong, M.-K.; Che, C.-M. Gold-mediated selective cysteine modification of peptides using allenenes. *Chem. Commun.* **2013**, *49* (14), 1428–1430.
- (29) Graf, N.; Lippard, S. J. Redox activation of metal-based prodrugs as a strategy for drug delivery. *Adv. Drug Delivery Rev.* **2012**, *64* (11), 993–1004.
- (30) Zhang, P.; Sadler, P. J. Redox-Active Metal Complexes for Anticancer Therapy. *Eur. J. Inorg. Chem.* **2017**, *2017* (12), 1541–1548.
- (31) Ryan, R. T.; Havrylyuk, D.; Stevens, K. C.; Moore, L. H.; Kim, D. Y.; Blackburn, J. S.; Heidary, D. K.; Selegue, J. P.; Glazer, E. C. Avobenzone incorporation in a diverse range of Ru(II) scaffolds produces potent potential antineoplastic agents. *Dalton Trans.* **2020**, *49* (35), 12161–12167.
- (32) Berners-Price, S. J.; Mirabelli, C. K.; Johnson, R. K.; Mattern, M. R.; McCabe, F. L.; Faucette, L. F.; Sung, C. M.; Mong, S. M.; Sadler, P. J.; Crooke, S. T. In vivo antitumor activity and in vitro cytotoxic properties of bis[1,2-bis(diphenylphosphino)ethane]gold(I) chloride. *Cancer Res.* **1986**, *46* (11), S486–S493.
- (33) Berners-Price, S. J.; Sadler, P. J. Interaction of the antitumor Au(I) complex [Au(Ph<sub>2</sub>P(CH<sub>2</sub>)<sub>2</sub>PPH<sub>2</sub>)<sub>2</sub>]Cl with human blood plasma, red cells, and lipoproteins: 31P an. *J. Inorg. Biochem.* **1987**, *31* (4), 267–281.
- (34) Sze, J. H.; Raninga, P. V.; Nakamura, K.; Casey, M.; Khanna, K. K.; Berners-Price, S. J.; Di Trapani, G.; Tonissen, K. F. Anticancer activity of a Gold(I) phosphine thioredoxin reductase inhibitor in multiple myeloma. *Redox Biol.* **2020**, *28*, 101310.
- (35) Reddy, T. S.; Privér, S. H.; Ojha, R.; Mirzadeh, N.; Velma, G. R.; Jaku, R.; Hosseinejad, T.; Luwor, R.; Ramakrishna, S.; Wlodkowic, D.; et al. Gold(I) complexes of the type [AuL{κC-2-C<sub>6</sub>H<sub>4</sub>P(S)Ph<sub>2</sub>}] [L = PTA, PPh<sub>3</sub>, PPh<sub>2</sub>(C<sub>6</sub>H<sub>4</sub>–3-SO<sub>3</sub>Na) and PPh<sub>2</sub>(2-py)]: Synthesis, characterisation, crystal structures, and In Vitro and In Vivo anticancer properties. *Eur. J. Med. Chem.* **2025**, *281*, 117007.
- (36) Schlagintweit, J. F.; Jakob, C. H. G.; Wilke, N. L.; Ahrweiler, M.; Frias, C.; Frias, J.; König, M.; Esslinger, E.-M. H. J.; Marques, F.; Machado, J. F.; et al. Gold(I) Bis(1,2,3-triazol-5-ylidene) Complexes as Promising Selective Anticancer Compounds. *J. Med. Chem.* **2021**, *64* (21), 15747–15757.
- (37) Long, Y.; Cao, B.; Xiong, X.; Chan, A. S. C.; Sun, R. W.-Y.; Zou, T. Bioorthogonal Activation of Dual Catalytic and Anti-Cancer Activities of Organogold(I) Complexes in Living Systems. *Angew. Chem., Int. Ed. Engl.* **2021**, *60* (8), 4133–4141.
- (38) Křikavová, R.; Hošek, J.; Vančo, J.; Hutýra, J.; Dvořák, Z.; Trávníček, Z. Gold(I)-triphenylphosphine complexes with hypoxanthine-derived ligands: in vitro evaluations of anticancer and anti-inflammatory activities. *PLoS One* **2014**, *9* (9), No. e107373.
- (39) Zhang, J. J.; Abu El Maaty, M. A.; Hoffmeister, H.; Schmidt, C.; Muenzner, J. K.; Schobert, R.; Wölfl, S.; Ott, I. A Multitarget Gold(I) Complex Induces Cytotoxicity Related to Aneuploidy in HCT-116 Colorectal Carcinoma Cells. *Angew. Chem., Int. Ed. Engl.* **2020**, *59* (38), 16795–16800.
- (40) Garcia, A.; Machado, R. C.; Grazul, R. M.; Lopes, M. T.; Corrêa, C. C.; Dos Santos, H. F.; de Almeida, M. V.; Silva, H. Novel antitumor adamantane-azole gold(I) complexes as potential inhibitors of thioredoxin reductase. *J. Biol. Inorg. Chem.* **2016**, *21* (2), 275–292.
- (41) Quero, J.; Ruighi, F.; Osada, J.; Gimeno, M. C.; Cerrada, E.; Rodríguez-Yoldi, M. J. Gold(I) Complexes Bearing Alkylated 1,3,5-Triaza-7-phosphaadamantane Ligands as Thermoresponsive Anticancer Agents in Human Colon Cells. *Biomedicines* **2021**, *9* (12), 1848.
- (42) Bian, M.; Sun, Y.; Liu, Y.; Xu, Z.; Fan, R.; Liu, Z.; Liu, W. A Gold(I) Complex Containing an Oleanolic Acid Derivative as a Potential Anti-Ovarian-Cancer Agent by Inhibiting TrxR and Activating ROS-Mediated ERS. *Chemistry* **2020**, *26* (31), 7092–7108.
- (43) Li, X.; Huang, Q.; Long, H.; Zhang, P.; Su, H.; Liu, J. A new gold(I) complex-Au(PPh<sub>3</sub>)<sub>3</sub>PT is a deubiquitinase inhibitor and inhibits tumor growth. *EBioMedicine* **2019**, *39*, 159–172.
- (44) Proetto, M. T.; Alexander, K.; Melaimi, M.; Bertrand, G.; Gianneschi, N. C. Cyclic (Alkyl)(Amino)Carbene (CAAC) Gold(I) Complexes as Chemotherapeutic Agents. *Chem. - Eur. J.* **2021**, *27* (11), 3772–3778.
- (45) Babgi, B. A.; Alsayari, J.; Alenezi, H. M.; Abdellatif, M. H.; Eltayeb, N. E.; Emwas, A. M.; Jaremko, M.; Hussien, M. A. Alteration of Anticancer and Protein-Binding Properties of Gold(I) Alkynyl by Phenolic Schiff Bases Moieties. *Pharmaceutics* **2021**, *13* (4), 461.
- (46) Chaves, J. D. S.; Tunes, L. G.; de J. Franco, C. H.; Francisco, T. M.; Corrêa, C. C.; Murta, S. M. F.; Monte-Neto, R. L.; Silva, H.;

- Fontes, A. P. S.; de Almeida, M. V. Novel gold(I) complexes with 5-phenyl-1,3,4-oxadiazole-2-thione and phosphine as potential anticancer and antileishmanial agents. *Eur. J. Med. Chem.* **2017**, *127*, 727–739.
- (47) Srinivasa Reddy, T.; Privér, S. H.; Rao, V. V.; Mirzadeh, N.; Bhargava, S. K. Gold(i) and gold(iii) phosphine complexes: synthesis, anticancer activities towards 2D and 3D cancer models, and apoptosis inducing properties. *Dalton Trans.* **2018**, *47* (43), 15312–15323.
- (48) Lu, Y.; Ma, X.; Chang, X.; Liang, Z.; Lv, L.; Shan, M.; Lu, Q.; Wen, Z.; Gust, R.; Liu, W. Recent development of gold(i) and gold(iii) complexes as therapeutic agents for cancer diseases. *Chem. Soc. Rev.* **2022**, *51* (13), 5518–5556.
- (49) Mertens, R. T.; Gukathasan, S.; Arojoye, A. S.; Olelewe, C.; Awuah, S. G. Next Generation Gold Drugs and Probes: Chemistry and Biomedical Applications. *Chem. Rev.* **2023**, *123* (10), 6612–6667.
- (50) Kim, J. H.; Ofori, S.; Parkin, S.; Vekaria, H.; Sullivan, P. G.; Awuah, S. G. Anticancer gold(iii)-bisphosphine complex alters the mitochondrial electron transport chain to induce in vivo tumor inhibition. *Chem. Sci.* **2021**, *12* (21), 7467–7479.
- (51) Arojoye, A. S.; Walker, B.; Dawahare, J. C.; Afrifa, M. A. O.; Parkin, S.; Awuah, S. G. Circumventing Physicochemical Barriers of Cyclometalated Gold(III) Dithiocarbamate Complexes with Protein-Based Nanoparticle Delivery to Enhance Anticancer Activity. *ACS Appl. Mater. Interfaces* **2023**, *15* (37), 43607–43620.
- (52) Gukathasan, S.; Parkin, S.; Awuah, S. G. Cyclometalated Gold(III) Complexes Bearing DACH Ligands. *Inorg. Chem.* **2019**, *58* (14), 9326–9340.
- (53) Mertens, R. T.; Kim, J. H.; Ofori, S.; Olelewe, C.; Kamitsuka, P. J.; Kwakye, G. F.; Awuah, S. G. A gold-based inhibitor of oxidative phosphorylation is effective against triple negative breast cancer. *Biomed. Pharmacother.* **2024**, *170*, 116010.
- (54) Kim, J. H.; Reeder, E.; Parkin, S.; Awuah, S. G. Gold(I/III)-Phosphine Complexes as Potent Antiproliferative Agents. *Sci. Rep.* **2019**, *9* (1), 12335.
- (55) Olelewe, C.; Kim, J. H.; Ofori, S.; Mertens, R. T.; Gukathasan, S.; Awuah, S. G. Gold(III)-P-chirogenic complex induces mitochondrial dysfunction in triple-negative breast cancer. *iScience* **2022**, *25* (5), 104340.
- (56) Arojoye, A. S.; Olelewe, C.; Gukathasan, S.; Kim, J. H.; Vekaria, H.; Parkin, S.; Sullivan, P. G.; Awuah, S. G. Serum-Stable Gold(III) Bisphosphine Complex Induces Mild Mitochondrial Uncoupling and In Vivo Antitumor Potency in Triple Negative Breast Cancer. *J. Med. Chem.* **2023**, *66* (12), 7868–7879.
- (57) Arojoye, A. S.; Mertens, R. T.; Ofori, S.; Parkin, S. R.; Awuah, S. G. Synthesis, Characterization, and Antiproliferative Activity of Novel Chiral [QuinoxP\*AuCl<sub>2</sub>]<sup>+</sup> Complexes. *Molecules* **2020**, *25*, 5735.
- (58) Mertens, R. T.; Jennings, W. C.; Ofori, S.; Kim, J. H.; Parkin, S.; Kwakye, G. F.; Awuah, S. G. Synthetic Control of Mitochondrial Dynamics: Developing Three-Coordinate Au(I) Probes for Perturbation of Mitochondria Structure and Function. *JACS Au* **2021**, *1* (4), 439–449.
- (59) Dennis, E. K.; Kim, J. H.; Parkin, S.; Awuah, S. G.; Garneau-Tsodikova, S. Distorted Gold(I)–Phosphine Complexes as Antifungal Agents. *J. Med. Chem.* **2020**, *63* (5), 2455–2469.
- (60) Gimeno, M. C.; Jones, P. G.; Laguna, A.; Laguna, M.; Terroba, R. Dithiolates as Bridging Ligands in Di- and Trinuclear Gold Complexes. X-ray Structures of [Au<sub>2</sub>(3,4-S<sub>2</sub>C<sub>6</sub>H<sub>3</sub>CH<sub>3</sub>)(PPh<sub>3</sub>)<sub>2</sub>], [Au<sub>2</sub>(1,3-S<sub>2</sub>C<sub>6</sub>H<sub>4</sub>)(PPh<sub>3</sub>)<sub>2</sub>], [Au<sub>3</sub>(3,4-S<sub>2</sub>C<sub>6</sub>H<sub>3</sub>CH<sub>3</sub>)(PPh<sub>3</sub>)<sub>3</sub>]-ClO<sub>4</sub>, and [Au(PPh<sub>2</sub>Me)<sub>2</sub>][Au(3,4-S<sub>2</sub>C<sub>6</sub>H<sub>3</sub>CH<sub>3</sub>)<sub>2</sub>]. *Inorg. Chem.* **1994**, *33* (18), 3932–3938.
- (61) Cerrada, E.; Jones, P. G.; Laguna, A.; Laguna, M. Synthesis and Reactivity of Heteroleptic Complexes of Gold with 2-Thioxo-1,3-dithiole-4,5-dithiolate (dmit). X-ray Structure of [Au<sub>2</sub>(μ-dmit)-(PPh<sub>3</sub>)<sub>2</sub>], (NBu<sub>4</sub>)[Au(dmit)(PPh<sub>3</sub>)], and (PPN)[Au(dmit)(C<sub>6</sub>F<sub>5</sub>)<sub>2</sub>]. *Inorg. Chem.* **1996**, *35* (10), 2995–3000.
- (62) Gimeno, M. C.; Laguna, A.; Sarroca, C.; Jones, P. G. 1,1'-Bis(diphenylphosphino)ferrocene (dppf) complexes of gold(I) and gold(III). Crystal structures of [(dppf)AuPPh<sub>3</sub>](ClO<sub>4</sub>).cntdot.CHCl<sub>3</sub> and [(dppf)Au(μ-dppf)Au(dppf)](ClO<sub>4</sub>)<sub>2</sub>.cntdot.2CH<sub>2</sub>Cl<sub>2</sub>. *Inorg. Chem.* **1993**, *32* (26), S926–S932.
- (63) Crespo, O.; Gimeno, M. C.; Laguna, A.; Jones, P. G. Two-, three- and four-co-ordinate gold(I) complexes of 1,2-bis-(diphenylphosphino)-1,2-dicarba-closo-dodecaborane. *Dalton Trans.* **1992**, No. 10, 1601–1605.
- (64) Vicente, J.; Arcas, A.; Jones, P. G.; Lautner, J. 2,4,6-Trinitrophenylgold(I) complexes. X-Ray crystal structures of [Au-(SbPh<sub>3</sub>)<sub>4</sub>][Au{C<sub>6</sub>H<sub>2</sub>(NO<sub>2</sub>)<sub>3</sub>-2,4,6}<sub>2</sub>]-Et<sub>2</sub>O and [Au{C<sub>6</sub>H<sub>2</sub>(NO<sub>2</sub>)<sub>3</sub>-2,4,6}(dmphen)](dmphen = 2,9-dimethyl-1,10-phenanthroline). *Dalton Trans.* **1990**, No. 2, 451–456.
- (65) Joost, M.; Zeineddine, A.; Estévez, L.; Mallet-Ladeira, S.; Miqueu, K.; Amgoune, A.; Bourissou, D. Facile Oxidative Addition of Aryl Iodides to Gold(I) by Ligand Design: Bending Turns on Reactivity. *J. Am. Chem. Soc.* **2014**, *136* (42), 14654–14657.
- (66) Sircoglou, M.; Mercy, M.; Saffon, N.; Coppel, Y.; Bouhadir, G.; Maron, L.; Bourissou, D. Gold(I) Complexes of Phosphanyl Gallanes: From Interconverting to Separable Coordination Isomers. *Angew. Chem., Int. Ed. Engl.* **2009**, *48* (19), 3454–3457.
- (67) Sircoglou, M.; Bontemps, S.; Bouhadir, G.; Saffon, N.; Miqueu, K.; Gu, W.; Mercy, M.; Chen, C.-H.; Foxman, B. M.; Maron, L.; et al. Group 10 and 11 Metal Boratranes (Ni, Pd, Pt, CuCl, AgCl, AuCl, and Au<sup>+</sup>) Derived from a Triphosphine–Borane. *J. Am. Chem. Soc.* **2008**, *130* (49), 16729–16738.
- (68) Zeineddine, A.; Estévez, L.; Mallet-Ladeira, S.; Miqueu, K.; Amgoune, A.; Bourissou, D. Rational development of catalytic Au(I)/Au(III) arylation involving mild oxidative addition of aryl halides. *Nat. Commun.* **2017**, *8* (1), 565.
- (69) Joost, M.; Amgoune, A.; Bourissou, D. Reactivity of Gold Complexes towards Elementary Organometallic Reactions. *Angew. Chem., Int. Ed. Engl.* **2015**, *54* (S0), 15022–15045.
- (70) Zou, T.; Lok, C.-N.; Wan, P.-K.; Zhang, Z.-F.; Fung, S.-K.; Che, C.-M. Anticancer metal-N-heterocyclic carbene complexes of gold, platinum and palladium. *Curr. Opin. Chem. Biol.* **2018**, *43*, 30–36.
- (71) Che, C.-M.; Sun, R. W.-Y. Therapeutic applications of gold complexes: lipophilic gold(iii) cations and gold(i) complexes for anticancer treatment. *Chem. Commun.* **2011**, *47* (34), 9554–9560.
- (72) Milne, J. E.; Buchwald, S. L. An Extremely Active Catalyst for the Negishi Cross-Coupling Reaction. *J. Am. Chem. Soc.* **2004**, *126* (40), 13028–13032.
- (73) Yang, Y.; Mustard, T. J. L.; Cheong, P. H.-Y.; Buchwald, S. L. Palladium-Catalyzed Completely Linear-Selective Negishi Cross-Coupling of Allylzinc Halides with Aryl and Vinyl Electrophiles. *Angew. Chem., Int. Ed. Engl.* **2013**, *52* (S2), 14098–14102.
- (74) Barder, T. E.; Walker, S. D.; Martinelli, J. R.; Buchwald, S. L. Catalysts for Suzuki–Miyaura Coupling Processes: Scope and Studies of the Effect of Ligand Structure. *J. Am. Chem. Soc.* **2005**, *127* (13), 4685–4696.
- (75) Old, D. W.; Wolfe, J. P.; Buchwald, S. L. A Highly Active Catalyst for Palladium-Catalyzed Cross-Coupling Reactions: Room-Temperature Suzuki Couplings and Amination of Unactivated Aryl Chlorides. *J. Am. Chem. Soc.* **1998**, *120* (37), 9722–9723.
- (76) Yang, Y.; Buchwald, S. L. Ligand-Controlled Palladium-Catalyzed Regiodivergent Suzuki–Miyaura Cross-Coupling of Allylboronates and Aryl Halides. *J. Am. Chem. Soc.* **2013**, *135* (29), 10642–10645.
- (77) Miyaura, N.; Yamada, K.; Suzuki, A. A new stereospecific cross-coupling by the palladium-catalyzed reaction of 1-alkenylboranes with 1-alkenyl or 1-alkynyl halides. *Tetrahedron Lett.* **1979**, *20* (36), 3437–3440.
- (78) Miyaura, N.; Suzuki, A. Stereoselective synthesis of arylated (E)-alkenes by the reaction of alk-1-enylboranes with aryl halides in the presence of palladium catalyst. *Chem. Commun.* **1979**, *19*, 866–867.
- (79) Arojoye, A. S.; Awuah, S. G. Functional utility of gold complexes with phosphorus donor ligands in biological systems. *Coord. Chem. Rev.* **2025**, *522*, 216208.

- (80) Abramson, V. G.; Lehmann, B. D.; Ballinger, T. J.; Pietenpol, J. A. Subtyping of triple-negative breast cancer: Implications for therapy. *Cancer* **2015**, *121* (1), 8–16.
- (81) Hongthong, K.; Ratanaphan, A. BRCA1-Associated Triple-Negative Breast Cancer and Potential Treatment for Ruthenium-Based Compounds. *Curr. Cancer Drug Targets* **2016**, *16* (7), 606–617.
- (82) Petrovic, N.; Davidovic, R.; Bajic, V.; Obradovic, M.; Isenovic, R. E. MicroRNA in breast cancer: The association with BRCA1/2. *Cancer Biomarkers* **2017**, *19*, 119–128.
- (83) Mittendorf, E. A.; Philips, A. V.; Meric-Bernstam, F.; Qiao, N.; Wu, Y.; Harrington, S.; Su, X.; Wang, Y.; Gonzalez-Angulo, A. M.; Akcakanat, A.; et al. PD-L1 expression in triple-negative breast cancer. *Cancer Immunol. Res.* **2014**, *2* (4), 361–370.
- (84) Beniey, M.; Hubert, A.; Haque, T.; Cotte, A. K.; Béchir, N.; Zhang, X.; Tran-Thanh, D.; Hassan, S. Sequential targeting of PARP with carboplatin inhibits primary tumour growth and distant metastasis in triple-negative breast cancer. *Br. J. Cancer* **2023**, *128* (10), 1964–1975.
- (85) Novohradsky, V.; Markova, L.; Kostrhunova, H.; Trávníček, Z.; Brabec, V.; Kasparkova, J. An anticancer Os(II) bathophenanthroline complex as a human breast cancer stem cell-selective, mammosphere potent agent that kills cells by necroptosis. *Sci. Rep.* **2019**, *9* (1), 13327.
- (86) Schirrmann, R.; Erkelenz, M.; Lamers, K.; Sritharan, O.; Nachev, M.; Sures, B.; Schlücker, S.; Brandau, S. Gold Nanorods Induce Endoplasmic Reticulum Stress and Autocrine Inflammatory Activation in Human Neutrophils. *ACS Nano* **2022**, *16* (7), 11011–11026.
- (87) Gallud, A.; Klöditz, K.; Ytterberg, J.; Östberg, N.; Katayama, S.; Skoog, T.; Gogvadze, V.; Chen, Y.-Z.; Xue, D.; Moya, S.; et al. Cationic gold nanoparticles elicit mitochondrial dysfunction: a multi-omics study. *Sci. Rep.* **2019**, *9* (1), 4366.
- (88) Zhang, Y.; Wu, Y.; Zhang, M.; Li, Z.; Liu, B.; Liu, H.; Hao, J.; Li, X. Synergistic mechanism between the endoplasmic reticulum and mitochondria and their crosstalk with other organelles. *Cell Death Discovery* **2023**, *9* (1), 51.
- (89) Li, R.; Luo, R.; Luo, Y.; Hou, Y.; Wang, J.; Zhang, Q.; Chen, X.; Hu, L.; Zhou, J. Biological function, mediate cell death pathway and their potential regulated mechanisms for post-mortem muscle tenderization of PARP1: A review. *Front. Nutr.* **2022**, *9*, 1093939.
- (90) Pandey, S.; Sharma, V. K.; Biswas, A.; Lahiri, M.; Basu, S. Small molecule-mediated induction of endoplasmic reticulum stress in cancer cells. *RSC Med. Chem.* **2021**, *12* (9), 1604–1611.
- (91) Ingle, J.; Tirkey, A.; Pandey, S.; Basu, S. Small-Molecule Endoplasmic Reticulum Stress Inducer Triggers Apoptosis in Cancer Cells. *ChemMedChem* **2023**, *18* (24), No. e202300433.
- (92) Parkin, S.; Hope, H. Macromolecular Cryocrystallography: Cooling, Mounting, Storage and Transportation of Crystals. *J. Appl. Crystallogr.* **1998**, *31* (6), 945–953.
- (93) Bruker AXS Inc. APEX3; Bruker AXS Inc.: Madison, Wisconsin, USA, 2012.
- (94) Sheldrick, G. Crystal structure refinement with SHELXL. *Acta Crystallogr.* **2015**, *71* (1), 3–8.
- (95) Sheldrick, G. A short history of SHELX. *Acta Crystallogr.* **2008**, *64* (1), 112–122.
- (96) Spek, A. L. Structure validation in chemical crystallography. *Acta Crystallogr., Sect. D: Biol. Crystallogr.* **2009**, *65* (2), 148–155.
- (97) Parkin, S. Expansion of scalar validation criteria to three dimensions: the R tensor. *Acta Crystallogr.* **2000**, *56* (2), 157–162.